A major purpose of the Technical Information Center is to provide the broadest dissemination possible of information contained in DOE's Research and Development Reports to business, industry, the academic community, and federal, state and local governments.

Although a small portion of this report is not reproducible, it is being made available to expedite the availability of information on the research discussed herein.

LA-UR--83-2847

DE84 001172

CONF-8310148--11

Los Alamos National Laboratory is operated by the University of California for the United States Department of Energy under contract W-7405-ENG-36.

TITLE: OPTICAL DIAGNOSTICS FOR CONDENSED-PHASE SHOCK-COMPRESSED MOLECULAR SYSTEMS

AUTHOR(S): S. C. Schmidt
D. S. Moore
J. W. Shaner

SUBMITTED TO: The CEA/Los Alamos High Explosives and Detonation Physics Conference, Paris, France, 3-6 October 1983

DISCLAIMER

Los Alamos National Laboratory
Los Alamos, New Mexico 87545

OPTICAL DIAGNOSTICS FOR CONDENSED-PHASE SHOCK-COMPRESSED MOLECULAR SYSTEMS*

S. C. Schmidt, D. S. Moore and J. W. Shaner

ABSTRACT

Experimental techniques capable of obtaining information about the molecular phenomenology in the region through and immediately behind the shockfront during the shock-compression of condensed-phase molecular systems are discussed and compared. Difficulties associated with performing measurements in this region are briefly reviewed. Some concomitant static experiments that can be used to complement the dynamic measurements are suggested. Developments and advances expected in diagnostic techniques during the next few years are summarized.

* Work supported by the US Department of Energy.

I. INTRODUCTION AND OBJECTIVES

Presently most hydrodynamics codes model explosive behavior by treating a heterogeneous explosive as an effective medium that is a continuum[1,2] (EMC) that chemically reacts according to either a pressure dependent or Arrhenius kinetics rate law. One or more parameters are used to incorporate the global chemical behavior, hydrodynamic phenomenology and effects of material heterogeneity. Essentially no effort is made to incorporate any of the microscopic details of the shock-compression/energy release phenomenology that constitutes the detonation process. In the past few years, several studies[3-8] have been started that attempt to improve the methodology of defining the EMC from a single component to one that incorporates ideas such as hot spots, voids or multicomponents. A short overview of these developments is given by Lee and Tarver.[3] Figure 1 conceptually depicts what we believe are the essential components of analytical models which can be used to describe detonation and shock-wave propagation in heterogeneous and homogeneous condensed-phase materials. Homogeneous materials are included because there is evidence to suggest that these materials do not remain hydrodynamically homogeneous during shock-compression.[9] The dotted line segment in Fig. 1 portrays current practices. In the future, statistical continuum theories[10] (SCT) may be used to generate the EMC. The degree of sophistication of the theory will reflect our level of understanding of the microscopic physical chemistry and fluid mechanic processes. Ideally, we would like to start with pure components and model the interactive behavior of these components with the medium. A more practical objective might be to understand and describe, using a SCT, the global behavior of explosive and binder decomposition and reaction in the heterogeneous hydrodynamic environment. There are several examples in the literature[11-18] of such theories being used to describe mechanical and electromagnetic wave progapation in heterogeneous materials.

Using an SCT to describe and model explosives will require considerably more experimental data than is available. For example, we would like to know to what "state" the explosive crystal and binder are being shock-compressed and what is the subsequent reaction history. Gauge experiments yield only thermodynamic parameters. Shock-recovery

experiments allow only a determination of the final products after expansion and cooling and give no direct information about the species immediately behind the shock front or reaction zone. Some of the optical techniques described in this paper potentially can be used to obtain this information. In particular we are hoping that Raman scattering, used in a clever fashion with appropriate test materials can be used to ascertain the structure and initial reaction steps of explosive crystals. Raman spectroscopy has already been used to make temperature estimates of shocked explosives.[18,19] Another example of data required to implement a SCT is the hydrodynamic behavior of heterogeneous materials. To our knowledge there are few or no experiments in progress which will provide information which can be used to construct a SCT prescription for explosives.

A nearer term application of molecular level optical diagnostic techniques is to attempt to understand the microscopic details of the energy transfer and chemical reaction paths followed by media during shock compression. With such information, it may be possible to specify and design particular reactive molecules for specific applications.

The goal of this paper is to discuss and evaluate experimental techniques that appear useful to determine the phenomenology through and immediately behind a shock-front during shock-compression of molecular systems. The phenomenology of particular interest is the microscopic physical and chemical behavior that occurs in this region and the coupling mechanisms of the microscopic processes to hydrodynamic and energy transport phenomena.

We have chosen to separate potential diagnostic techniques into four categories: (1) those that contribute directly to deducing phenomenology from a real-time measurement in the region of interest; (2) those that contribute indirectly in that phenomenology is inferred from measurements made outside the domain of interest; (3) complementary experiments on non-shock-compressed systems and (4) those experiments whose results cannot be used to determine phenomenology but serve as constraints in modeling behavior. Historically, most diagnostic techniques for studying condensed phase shock-wave phenomena have fallen into categories two and four. In this

discussion we will focus primarily on category one: direct realtime measurements through and immediately behind the shock-front. Possible complementary measurements at high pressure and temperature, i.e. category 3, will also be discussed because such results are useful in the interpretation of category 1 experiments and may serve to elucidate some of the unique features of the shock-front.

II. EXPERIMENTAL CONSIDERATIONS

Prior to discussing diagnostic techniques, several problems associated with conducting condensed-phase shock-wave experiments will be reviewed. These difficulties have historically limited the ability to conduct experiments in the adverse conditions through and immediately behind the shock-front. The success of any technique can probably be measured in its ability to circumvent one or more of these problems.

For many materials shock waves are believed to be of the order of 1 μ or less in thickness.[20,21] The passage time through the front of a 1 μ-thick shock whose velocity is 5 km/sec is thus of the order of 200 psec or less. Hence, if we desire to temporally and spatially resolve a measurement through a shock-front (5 data points), the diagnostic technique selected must be capable of spatial and temporal resolutions of 0.2 μ and 40 psec, respectively. Condensed-phase chemical reaction times can be of the order of 1 psec, thus necessitating even better temporal resolution. However, if all that is desired is to resolve features in the few mm long region behind the shock-front where relaxation and reaction processes may occur, then these requirements are drastically reduced.

Optical techniques offer some potential for achieving measurements within these stated limitations. However, with such methods some additional complications arise. Many materials are opaque or become opaque when shock-compressed. Consequently, the use of optical diagnostic techniques will be limited to a few select materials primarily for phenomenology studies. Such studies may, however, have tremendous potential when used in conjunction with other techniques for determining phenomenology of shock-compressed materials. Two other difficulties inherent in optical shock-

wave diagnostic techniques are the changes in material refractive index that accompany the density changes characteristic of shock waves and the possibility of photochemistry induced by the optical probes. Figure 2 shows the path deviation that occurs when an optical beam is passed through a shock-compressed system. The trailing shock wave near the sample boundaries tends to bend the optical beam away from the shock-front thus making prediction of the expected optical path difficult. Any shock-front curvature will compound this difficulty. If the shock velocity in the windows is greater than in the sample, additional complications could arise from the effect of the more complex wave structure on window transmission. Many molecules undergo photochemical reactions when exposed to light, particularly that in the ultraviolet region of the spectrum. If these reactions are fast compared to the characteristic time of the optical diagnostic, measurements could include the effects of both the shock stimulus and the photochemical reaction.

Measurements made using inhomogeneous samples often are averages over the nonuniformities and consequently do not reflect the details of the microstructure. For materials like granular explosives, the inhomogeneous nature is readily apparent and experiments are interpreted accordingly. For samples thought to be homogeneous, ambiguities can arise. For example, Fig. 3 depicts two image-intensifier-camera pictures [9] of the shock-front of detonating nitromethane and an 80% nitromethane/20% acetone mixture. Liquids are often thought to be homogeneous materials. However, these pictures show that microstructure exists in the vicinity of the shock-front. Also, nothing is known about microstructure in the region immediately behind the shock front. When performing experiments on nitromethane or similar substances, especially experiments utilizing optical techniques where a spatial resolution of tens of microns is desired, one must be aware that results may actually reflect an average over a smaller characteristic microstructure. Conversely, a single measurement with spatial resolution smaller than the microstructure may be misinterpreted as representative of the average material.

Shock recovery experiments are often used to observe chemical and physical changes through and immediately behind the shock-front. However, these changes occur not only in the high pressure and temperature region at the shock front, but also in the somewhat lower pressures and temperatures in the expansion region. Inability to separate these two effects makes the interpretation of these experiments difficult.

III. DIAGNOSTIC TECHNIQUES

In this section we will discuss several established and potentially useful diagnostic techniques which can be used to study the behavior of shock-compressed molecular systems. As stated previously, those experiments that yield results elucidating microscopic phenomenology through and immediately behind the shock-front will be emphasized. Other established methods, such as shock recovery, conductivity and gauge techniques, are well known historically.

A. Direct Techniques

Two methods have been identified as potentially capable of having either sufficient temporal or spatial resolution for measurements in the shock-front region: (1) Fast Optical Spectroscopic and Scattering Techniques and (2) Pulsed X-Ray Techniques. Because sub-nanosecond coherent x-ray sources capable of probing a shock front are still to be developed, the optical methods are the most realizable in the near future.

1. Optical Methods

a. Absorption/Emission Spectroscopy. Emission spectroscopy of condensed-phase shock-compressed chemically reacting and inert materials has been reported by many authors. These measurements have been used both to determine temperatures[20,22-33] and to identify spectral features[20,24,27,34-38] resulting from shock-compression. Other investigations of emission during shock-compression have been reviewed by Davison and Graham.[40]

Calculation of temperature using either the brightness or the multi-color method usually requires additional knowledge and assumptions about the emissivity and optical depth of the radiating sources. Failure to recognize this can result in an incomplete interpretation of the observed phenomenon. For example, as shown in Fig. 4 a 6,000 K black body source viewed through a 4,000 K black body will not be observed since the radiation is absorbed and re-remitted at the temperature of the intervening layer. This effect has been observed[20,26] during the shock-compression of ionic crystals. Figure 4 also shows results of changing the emissivity of the 4,000 K layer from 1.0 to 0 and 0.9. Radiation measured in the case of emissivity equal to 0.9 could easily be misinterpreted as originating from a 4,650-K black body. Brightness and color temperatures, as observed in a series of experiments using shock-compressed plastic bonded explosive (PBX) 9404,[30,31] could also be incorrect because of surface inhomogeneities similar to those depicted in Fig. 3.

To date, most observed emission spectra have been grey-body in character, however, in some cases, both for inert and reacting materials, spectral features which differ from grey-body radiation have been detected. Triboluminescence and non-grey-body radiation have been observed for shock-compressed quartz[20,27,34,35] and other materials.[28] Spectral features have been noted for shock-compressed 1,3,5-trinitro-1,3,5 triazacyclohexane (RDX)[24,36] and pentaerythritol tetranitrate (PETN).[37,38] For the RDX observations, complementary Raman scattering[36] measurements aided in interpretation of the data. Generally the potential for emission spectroscopy has not been fully exploited.

In order to use emission spectroscopy for determining phenomenology through and immediately behind the shock-front, two major obstacles must be overcome. First, an experiment with adequate time resolution must be devised. As was discussed previously, a temporal resolution of 40 psec is probably necessary for shock fronts. This resolution may be achieved using electronic streaking cameras. Second, a method of separating shock-front emission from background radiance must be found. Figure 5 suggests a possible experiment. Here, as the shock-front progresses from the opaque into the transparent materials, the transparent material can be viewed as

shocked radiating layers building up one at a time. Techniques exist[40,41] for interpreting emission spectra from such sources, providing a measurement can be made as each new layer is added. Even though emission intensities can be expected to be small for relatively thin optical depths, existing electronic streaking cameras equipped with intensifiers may be capable of recording the emission with more than adequate time resolution. Such emission spectra should yield features useful for the deduction of the microscopic phenomenology through the shockfront. Some advantages and difficulties of emission spectroscopy are given in Table I.

Absorption spectroscopy measurements of shock-compressed materials have been used to study mechanisms of light absorption[20,25-49] index of refraction changes,[20,40,50-54] and the shift of absorption bands during shock-compression.[55-61] Davison and Graham[40] have recently reviewed experiments which measure changes in the refraction index. Generally, absorption measurements have been performed in the visible and ultraviolet regions of the spectrum using instruments of relatively low dispersive power. Figure 6 shows the absorption experiments used by Duvall et al.[57-61] Two techniques, one with the flashlamp light source located in the projectile and one with the reflecting surface removed from shock effects, represent improvements over previously used methods. During the experiment absorption occurs primarily in the steady-state region behind the shock front and the shift of the absorption bands is assumed to occur immediately on passage through the shock-front. Shifts in absorption bands can be used to infer changes in molecular energy levels. However, interpretation can be difficult since the details of vibronic state energy levels are complex and may not be understood. If, in such an experiment, spatially resolved measurements are desired through and in the region immediately behind the shock front, knowledge of pressure, temperature, density and reaction phenomenology along the absorption path must be used to deconvolute the spectra. Ewald and David[44-45] have observed spatially resolved changes behind the shock front of the absorption spectra of uranyl chloride solutions using the experimental configuration depicted in Fig. 3. Spatial resolution was ± 1 mm.

Molecular vibrational transitions occur in the infrared region of the spectrum where sensitive fast detection systems are not yet available. Techniques employing stimulated electronic Raman scattering down conversion of short pulse length broadband visible radiation to longer wavelengths for use as a broadband infrared absorption source and then stimulated electronic Raman scattering and parametric up conversion of the transmitted signal to the visible for detection may be usable for fast infrared absorption spectroscopy of shock-compressed materials. The system developed by Bethune et al.[62-64] is shown in Fig. 7. Spectral and temporal resolutions achieved are 0.5 cm^{-1} and 10 nsec respectively. Adopting this technique to shock wave studies would require transmission and reflection of the infrared beam in shocked materials or through shocked windows. Other advantages and disadvantages for absorption spectroscopy are given in Table I.

b. Luminescence. We include in this category all forms of light emission from a material in which thermal energy is not the mechanism of excitation to the radiating state. Electroluminescence is luminescence resulting from strong-electric-field acceleration of electrons or ions to optical energies.[20,65-68] Chemiluminescence results when energy released in a chemical reaction is radiated as light. In a detonation or shock-compression induced chemical reaction, the luminescence might appear as an increased intensity above that expected from a black body spectrum.

Another form of luminescence, triboluminescence[20,35,66] is thought to result from the fracturing of material; it may be an electroluminescence effect. Luminescence has also been observed in shock-compressed porous solids.[67,69-71] The large strains induced by shock waves can also produce transient localized effects, such as compressing trapped gases to temperatures above those of the surrounding material.[71] Such an effect would yield radiation intensities in excess of the black body levels based on the material temperature. Reported observations of luminescence from shock-compressed materials resulting from any of the above effects have received limited use for ascertaining the phenomenology during shock-compression. Perhaps better temporal and spatial resolution of the emitted radiation would aid interpretation.

Fluorescence is emission subsequent to excitation by the absorption of light. Phosphorescence is the name given to the fluorescence which continues, primarily due to a forbidden decay process, long after excitation has ceased. Fluorescence is frequently used as a diagnostic to st intra- and inter-molecular collisionally activated processes and to measure relaxation rates[72] for vibronic and vibrational states. Current techniques use lasers as exciting sources to selectively populate a single energy level. Fast emission spectroscopy is then used to monitor the population in the initially excited energy level, as well as the manifold of states to which the excited state converts by collisional or unimolecular processes (Fig. 8). The character of the emission band is determined by the intramolecular relaxation or the internal conversion time and the radiative lifetime of the pertinent states. Data interpretation can be complicated. A useful variation of this technique is optical-optical double-resonance spectroscopy.[73] For example, an initial infrared pulse can be used to excite a vibrational level in the ground electronic state. A second laser pulse, temporally delayed with respect to the first, excites the molecule to an energy level in a higher electronic state. The relaxation of the intermediate level is mapped out by monitoring the intensity of emission of the higher electronic state as a function of the delay time between the two excitation pulses.

To date, fluorescence and phosphorescence techniques have been used to study materials under static high pressure[74] but have not been applied to condensed-phase shock-compressed systems. Fluorescence may be a good method for determining intra- and inter-molecular energy transfer mechanisms for vibronic states (Table I). Emission intensities, although not as large as the beam intensities of the coherent scattering techniques to be discussed below are sufficiently strong to be observed using picosecond techniques. Discrimination against a bright thermal background may also complicate their use in shock-wave applications. Double resonance techniques, if usable, would produce signals only where the beams overlap and consequently would permit better spatial resolution.

c. Spontaneous Raman Spectroscopy in shock-compression systems was first performed in detonating crystalline RDX.[37] Subsequently the technique has been used to measure the temperature of detonating nitromethane[19,75] and to look at the frequency shifts of vibrational bands of detonating PETN and RDX.[76,77] A Raman scattering measurement has recently been performed in water that was shock-compressed using a high velocity gas gun.[78]

Raman scattering is the inelastic scattering of light from molecules (Fig. 9). The scattering cross-section and hence the detection sensitivity are considerably smaller than for dipole emission/absorption processes (see Table II). The small scattering cross-section becomes particularly relevant when the scattering medium has a large background emission level such as might be true in a hot shock-compressed material. This difficulty can be overcome to some degree by using a short wavelength exciting frequency; however, care must be taken to avoid interfering fluorescence from photochemically produced species.

Since Raman scattering occurs into 4 π steradians, detection can be made at an angle to the exciting beam so that spatial resolution is determined by either the diffraction limit of the optical components or the sensitivity of the detector and the magnitude of the scattering cross-section. This is a significant advantage compared to dipole emission/absorption techniques where the observed light results from emission/absorption along a path length. Temporal resolution is limited by the sensitivity of the detector, the pulse duration of the exciting laser and the magnitude of the scattering cross-section. Figure 10 shows schematically the Raman scattering experiments[75-77] used to measure temperatures via Stokes-anti-Stokes intensity ratios and vibrational frequency shifts for shock-compressed and detonating energetic materials. An explosively driven plane wave generator was used to generate a shock in the sample. A pin signal in conjunction with a time delay was used to Q-switch the laser after the shock-front had traveled a few mm into the sample. The laser pulse was directed into the sample normal to the shock front. For both experiments scattering was observed at 90° to the incident exciting radiation. Timing accuracy of the laser pulse with respect to passage of the shock front was of the order of 0.1 μs. The information that can be gained from these

kinds of experiments is primarily the shifts in molecular energy levels resulting from shock-compression and an estimate of the vibrational temperature in the region behind the shock front. Although good spatial resolution is possible, these experiments will have difficulty because the refractive index effects discussed earlier make precise optical alignment difficult. In addition, the small signal intensities, particularly when viewed against high emission backgrounds, will limit the ability of Raman scattering to detect species with small concentrations. Advantages and disadvantages of spontaneous Raman scattering are given in Table II.

Resonance Raman scattering occurs when the exciting frequency is in resonance or near resonance with an actual electronic transition of the system.[79,80] For discrete and continuum resonance Raman scattering, the scattered intensity can increase dramatically both for fundamentals and overtones and selective resonance enhancement can occur for select species. Emission lifetimes from excited states can also become long due to the onset of resonance fluorescence. In addition, since laser radiation is being absorbed by the sample, complications from photochemistry and sample heating can be expected. Time resolved nsec and psec resonance Raman spectroscopy experiments[80,81] have been performed at ambient conditions. Generally signal averaging was used to improve signal-to-noise ratios. Results of single pulse experiments[80] while improved compared to spontaneous Raman scattering intensities, do not show particularly good signal-to-noise ratios. Pulsed resonance Raman scattering measurements may be possible in shock-compressed systems to determine vibrational overtones if the actual electronic transitions are known, however, gating of the detector might be required to eliminate fluorescence effects. Under shock-compression this technique would also suffer from the same alignment and timing difficulties as spontaneous Raman scattering experiments (Table II).

d. Coherent Raman Spectroscopy. Several coherent Raman scattering techniques are available (Fig. 11). Advantages of these techniques, primarily because of large scattering intensities and the beam like nature of the scattered signal (Table II) are increased detection sensitivity, temporal resolution limits approaching laser pulse lengths and possible spatial resolution approaching the diffraction limit of the optical compo-

nents. As with using all optical methods in shock-wave applications, optical accessibility because of material opacity or particulate scattering remains a major difficulty with the coherent Raman techniques.

Backward-stimulated Raman scattering (BSRS) has been observed in shock-compressed benzene.[82] Stimulated Raman scattering[83,84] (Fig. 11) occurs when the incident laser intensity in a medium exceeds a threshold level and generates a strong, stimulated, Stokes beam. The threshold level is determined by the Raman cross-section and linewidth of the transition and by the focusing parameters of the incident beam. Typical threshold intensities are ~10-100 GW/cm^2. Figure 12 illustrates the arrangement used for a backward stimulated Raman scattering experiment. An aluminum projectile of known velocity from a 51-mm-diam 3.3-m-long gas gun impacted an aluminum target plate producing a shock wave which ran forward into a 9 to 11-mm-thick benzene sample. Standard data reduction techniques[85] using published shock-velocity/particle-velocity data[86] were used to determine the state of the shock-compressed benzene. A single 6-ns-long frequency-doubled Nd-doped yttrium aluminum garnet (Nd:YAG) laser pulse was focused through the quartz window to a point in the benzene 2 to 6 mm in front of the rear sample wall. The timing sequence was determined by the incoming projectile. Interruption of a HeNe laser beam, in conjunction with an appropriate time delay, triggered the laser flash lamp approximately 300 μs prior to impact. A time-of-arrival pin activated just before impact and the appropriate time delay served to Q switch the laser just prior to the shock wave striking the quartz window and after it was well past the focal point of the incident laser light.

In liquid benzene, the ν_1 symmetric stretching mode[87] at 992 cm^{-1} has the lowest threshold for stimulated Raman scattering induced by 532-nm light, and was the transition observed in these experiments. As depicted in Fig. 11, the backward stimulated Raman beam was separated from the incident laser by means of a dichroic filter and was then focused onto the 10-μ-wide entrance slit of a 1-m Czerny-Turner spectrograph equipped with a 1200-grooves/mm grating used in first order. Figure 13 shows the resulting spectrogram for benzene shock-compressed to 0.92 GPa. The reflected incident laser line and the backward stimulated Brillouin-scattering line

at 532 nm are observable, as are the backward stimulated Raman-scattering line from the shocked sample and the backward stimulated Raman-scattering line from ambient benzene. The latter feature resulted as a consequence of the shock wave having passed only about two-thirds of the way through the sample, and hence a stimulated Raman signal was also obtained from the unshocked liquid.

The frequency shift of the Raman line has small contributions of approximately 0.1 cm^{-1} because the light crosses the moving interface between two media of different refractive indices and because of the material motion behind the shock wave.[88] Since these errors are considerably less than the experimental uncertainty of $\pm$ 0.5 cm^{-1} for the measured frequency shifts and are a small fraction of the shift due to compression, no attempt was made to correct the data for these effects.

Figure 14 gives the measured shift of the ν_1 ring-stretching mode vibrational wave number versus pressure of the shocked benzene. Observation of the ring-stretching mode at 1.18 GPa strongly suggests that benzene molecules still existed several millimeters behind the shock wave at this pressure, but does not, however, exclude some decomposition.[89]

Signal beam intensities using BSRS are sufficiently large that film can be used as a detector. The large incident intensities required, however, can cause damage to optical components near focal points. Spatial and temporal resolution (Table II) are determined by the confocal parameter of the focusing lens and the incident laser pulse duration. The BSRS technique also suffers because only certain molecules produce stimulated Raman scattering and of these molecules only the lowest threshold transition can be observed. Therefore, stimulated Raman scattering is probably best used as a diagnostic to look at single select species in the steady region behind the front of a supported shock.

Inverse Raman or stimulated Raman loss spectroscopy[90,91] (Fig. 11) has been suggested[92] and used as a diagnostic technique for shock-compressed systems. Scattering can occur at incident power levels considerably below those required for stimulated Raman scattering by overlapping the pump beam

with a beam, usually a broadband source, at the anti-Stokes frequency. Radiation is scattered from the broadband source (appears as an absorption) into the pump frequency. No threshold intensity exists as in the case of stimulated Raman scattering. Hence, the complete Raman-active spectrum, with sufficient intensity to overcome fluorescence and other background effects, should be visible.

Since phase matching is not required as in many of the coherent techniques discussed later, several geometric arrangements are possible. Figure 15 shows a schematic of an inverse Raman experiment used to measure vibrational frequency shifts in shock-compressed cyclohexane, nitromethane and single crystal PETN.[33] Spatial and temporal resolution (Table II) should be the diffraction limit of the optical components and the laser pulse length, respectively. A difficulty does arise with the inverse Raman technique when a broadband dye laser is used for the anti-Stokes beam. Roughness or irregularities in the intensity of the continuum, due mostly to etalon behavior of the optics in the laser and thermal gradients in the dye stream, can be of the order of the absorption signal, thus adversely affecting spectral resolution and detection sensitivity.

Coherent anti-Stokes scattering (CARS) and coherent Stokes Raman scattering (CSRS)[93,94] (Fig. 11) occur as four-wave parametric processes in which three waves, two at a pump frequency ω_p and one at either the Stokes, ω_s, or anti-Stokes ω_{as} frequency are mixed in a sample to produce a coherent beam at the anti-Stokes or Stokes frequency, respectively. The mixing is greatly enhanced if the frequency difference between the pump and the Stokes or anti-Stokes frequencies coincides with a Raman active mode of the sample. Like inverse Raman scattering, CARS and CSRS can be produced at incident power levels considerably below those required for stimulated Raman scattering. However, since phase matching is required, possible geometrical arrangements are limited.

Figure 16 depicts a CARS experiment in shock-compressed liquid benzene and mixtures of benzene and perdeuterobenzene (benzene-d_6).[95] The gas gun described previously was used to accelerate a magnesium projectile with an 8-mm thick, 304 stainless steel warhead to a desired velocity. The projec-

tile struck a 2.1-mm thick 304 stainless steel target plate producing a shock wave which ran forward into a 7.5 to 8.0-mm thick benzene (or mixture) sample. Stainless steel was chosen because previous experience has shown it to retain its reflectivity under shock compression. The state of the shock-compressed samples was again determined using published shock-velocity/particle-velocity data.[86] Mixture densities were determined according to volume fraction of benzene and benzene-d_6. The timing sequence for the reflected broadband CARS (RBBCARS) experiment differed from that of BSRS experiments in that aluminum time-of-arrival pins replaced the HeNe laser beam triggering system. Since the Raman frequencies of the shock-compressed materials are not precisely known, and since we wished to produce CARS signals from more than one mode or species, a broad-band dye laser, with a bandwidth equivalent to the gain profile of the dye, was used as the Stokes beam.[96] A portion of the 6 ns long frequency doubled Nd:YAG laser pulse was used to pump the dye laser. The resulting two laser beams (dye and remaining pump) were passed through separate Galilean telescopes and sent along parallel paths towards the sample. The beams were focused and crossed (with approximately 1 mm length of overlap) at a point approximately 4 mm in front of the rear sample wall using a previously described technique.[97] The beam crossing angle (phase-matching angle) was tuned by adjusting the axial distance between the parallel beams using a precision translation stage on the dye laser beam turning prism. The CARS beam was reflected out of the shocked sample by the highly polished front surface of the target plate and along a path parallel to the two incoming beams. After being separated from the pump and Stokes beams using a long-wave-length-pass dichroic filter, the beam was then passed through a dove prism and focused onto the 75 μm wide entrance slit of the spectrometer. The dove prism was used to rotate the image of the CARS signal so that any beam movement resulting from the changing position of the reflecting surface during the shock-compression process would translate to movement along, rather than across, the spectrometer entrance slit. The signals were detected at the exit of the spectrometer using a silicon-intensified-target vidicon (EGG-Par 1205D) coupled to an optical multi-channel analyzer (OMA) (EGG-PAR 1205A).

Figure 17 shows the OMA recorded RBBCARS signals for the ring-stretching modes of benzene and benzene-d_6 in a 60% benzene, 40% benzene-d_6 (by volume) mixture, both at ambient conditions and shock-compressed to 0.91 GPa. Also shown is the 253.652 nm Hg line in second order used as a wavelength reference. The spectral data obtained using RBBCARS shows no evidence for the presence behind the shock of decomposition product species[89] (at concentrations above the 10-20% level) having Raman active transitions within the vibrational frequency region spanned by the gain profile of the dye (i.e., between 800 and 1100 cm^{-1}). In addition, the spectra obtained for the mixtures do not contain any evidence for deuterium exchange reactions between the benzene species during the ~1 μs after passage of the shock. If exchange had occurred, new peaks would be evident between the benzene and benzene-d_6 transitions. Measured vibrational ring-stretching frequency shifts for benzene obtained using RBBCARS and the shifts measured using BSRS as a function of shock pressure are shown in Fig. 14. The data indicate that the two techniques measure equivalent frequency shifts at equivalent shock pressures. Temporal resolution for the RBBCARS technique is determined by the laser pulse duration. Since the beam crossing-angles required for phase matching are a few degrees, spatial resolution is somewhat less than the confocal parameter of the focusing lens (Table II). This decrease in spatial resolution from that potentially available with inverse Raman scattering is a distinct disadvantage of CARS and CSRS, and will ultimately be a handicap when trying to measure relaxation phenomena in the region immediately behind the shock front.

The real advantage of CARS and CSRS experiments is the large scattering intensity and beam-like nature of the signals that enable tremendous discrimination against background fluorescence and emission. CARS also frequency discriminates against fluorescence interference. By proper sample selection, interference from the non-resonant background signals and cross-talk between closely spaced lines can be minimized. Because of the large signal-to-noise ratios expected, detection of species with concentrations down to part-per-hundred levels should be possible.

A second RBBCARS geometry called reflected-broadband "BOX" coherent anti-Stokes Raman scattering[98] (RBBBOXCARS) is presently being attempted in a shock-compressed material. For RBBBOXCARS the two pump beams in the four wave mixing process are brought together at some angle rather than being collinear. If this technique is successful, the spatial resolution possible will increase considerably from that achieved with RBBCARS.

Raman-induced Kerr effect spectroscopy (RIKES)[99] has been suggested as a diagnostic technique[92] for performing measurements in shock-compressed systems which may have a large non-resonant background. Similar to inverse-Raman scattering, RIKES requires a single frequency pump beam, a broad-band probe source, no phase matching and lower incident power levels than stimulated Raman scattering (Fig. 11). Appropriate polarization of the input pump and probe beams results in a scattered probe beam whose polarization is rotated at conditions of Raman resonance. An analyzer placed in the scattered probe beam thus transmits light only at differences in frequency corresponding to Raman resonances. This arrangement ideally would give a large signal intensity against a small background making it a good choice for the detection of species with small concentrations. In shock applications, however, two difficulties could arise. The strained shock-compressed sample could exhibit birefringence that would rotate the polarization of all of the incident probe frequencies, resulting in a large unwanted background. The second problem arises in geometric arrangement considerations. Since a polarization analyzer is required in the output beam, a straight line transmission arrangement is the most logical choice (Fig. 15). A second choice, shown in Fig. 18 uses an apparatus very similar to the RBBCARS apparatus.[100,101] The portion of the frequency-doubled Nd:YAG laser beam that does not pump the dye laser is passed through a Fresnel rhomb to produce a beam of >99% circular polarization. The dye laser beam (Stokes frequencies) is passed through a high quality Glan-Taylor (air-gap) prism to produce a beam of ~1 part in 10^6 linear polarization. The two beams are focused and crossed in the sample at an angle near 6 degrees, giving an overlap length of ~150 μm at the focus. The Stokes beam is then reflected by the highly polished front surface of the target plate back through the sample and along a path parallel to the incoming beams. A mirror separates the reflected dye laser beam from the

other beams and directs it first through a Babinet-Soliel polarization compensator and then through a Glan-Taylor polarization analyzer. The compensator was found to be necessary to remove the ellipticity introduced into the linearly polarized Stokes laser beam by the birefringence inherent in the optical components located between the polarizers, including the ambient sample. When the two Glan-Taylor prisms are crossed, the dye laser beam is blocked except at frequencies corresponding to Raman resonances, where the RIKES signals are passed. These signals are directed through the dove prism, focused into the entrance slits of the 1 m spectrometer and detected by the OMA system. If the crossing angle is increased, temporal and spatial resolutions for such an arrangement should be the laser pulse length and the diffraction limit of the optical components used.

Figure 19 shows two RIKES 992 cm^{-1} region spectra of benzene shock-compressed to 1.17 GPa. Both traces have spectral features, however they are not consistent and do not exhibit the pressure-induced frequency shift expected for the benzene ring stretching mode based on previous BSRS and RBBCARS experiments. In addition the broadband signal at the dye frequency suggests a shock-induced polarization rotation of the entire probe beam. The conclusion reached from these experiments is that while it may be possible to perform RIKES in shock-compressed materials, the experiment will be considerably more difficult than techniques not sensitive to the absolute polarization of the laser beams. (Table II).

If the output beam of a parametric mixing process is sufficiently strong, it can further mix with one of the incident beams and create a new output beam at yet a different frequency. Higher order Raman spectral excitation studies (HORSES) (Fig. 11) have been used to generate coherent second Stokes and second anti-Stokes beams. Other multi-color parametric mixing processes using polarized beams have been used to observe Raman transitions. These techniques are generally used to suppress non-resonant background effects. Observation of any of these more complicated processes in shock-compressed systems will probably come after some of the techniques discussed previously are further developed. Optical alignment for any technique dependent on polarization effects will surely be quite difficult.

e. Brillouin Scattering and Reflection Experiments. Brillouin scattering[102,104] is the inelastic scattering of light from isentropic density fluctuations or acoustic waves in a transparent medium. It is therefore a probe of the low frequency excitations of the system, in contrast to Raman scattering. The frequency shift of the scattered light is dependent on the velocity of the acoustic wave and the scattering angle. Similar to the ordinary Raman effect, the scattering amplitude is small and, since the frequency shift is also small, observation of Brillouin scattering without a laser excitation source is extremely difficult. In a milestone experiment, Keeler et al.[88,105] used the coherent scattering of light from acoustic waves, or backward stimulated Brillouin scattering, to measure sound velocities in shock-compressed water and acetone. The experimental arrangement is similar to that shown in Fig. 12 for backward stimulated Raman scattering, only the spectrograph is replaced by an interferometer and Fabry-Perot interferograms are obtained in place of spectrograms. Interpretation of Brillouin scattering data for shock-compressed systems requires two corrections; one because the material particle velocity behind the shock wave results in a Doppler frequency shift of both the incident and scattered beams and a second because both the incident and scattered beams pass through a moving density or index of refraction gradient in the shock front. The frequency shift for both of these corrections is of the same magnitude as the Brillouin shift.

Reflection of visible wavelength light has been used to determine the index of refraction of shock-compressed materials[20,106-108] and to qualitatively examine the surface roughness of shock and detonation waves.[20,109] Generally, measurements performed with shock waves whose thicknesses are much less than the wave length of the incident light give values for the index of refraction of the shock-compressed material which are comparable to those measured using geometric methods. When the shock-wave thickness or surface roughness approaches the wave length of the incident light a more complex treatment is required to interpret reflectance measurements.

The index of reflection of molecular dielectrics is determined by the electrical polarizibility of the material. The direct connection between shock-induced polarization and chemical activity and mechanical deformation

processes through the shock front is still ambiguous.[110] Because electrical or index-of-refraction measurements are bulk property values which can average over several microscopic effects, these kinds of experiments will most likely require complementary information describing the structure, energy transfer, and chemical activity resulting from shock-compression. Once some details of the microscopic processes are known, associations to the optical and electrical behavior will enable a more complete and beneficial interpretation of these results.

Short Wavelength Diffraction Methods. Short wavelength techniques offer two distinct advantages when compared to most other diagnostics used to explore shock-compression phenomenology: first, short wavelength radiation in the form of x-rays or energetic electrons will penetrate normally opaque materials and second, the short wavelength radiation offers a potential spatial resolution of the order of the radiation wavelength. Johnson et al.[111-115] and other investigators[116-120] have used flash x-ray diffraction (FXD) to determine structural changes in situ for materials subjected to large stresses as a result of either shock compression or shaped charge jet formation. In the experiment (Fig. 20) done at Lawrence Livermore National Laboratory, an x-ray beam incident on the surface of the material to be studied is discharged simultaneously with the arrival at the surface of an explosively driven shock front. This simultaneity was necessary as the penetration depth was small. The scattered radiation, reflecting crystal structure changes, is recorded at the Bragg angle using either a scintillation detector[121] or a film cassette.[122] Minimum x-ray pulse width achieved was of the order of 50 nsec. A major difficulty encountered with the experiment was the inability to discharge the Blumlein x-ray source with sufficient timing accuracy to insure consistent synchronization with the shock-wave arrival at the sample surface. Sawaoka,[123] et al. are presently working on a technique to improve the timing accuracy of their experiments.[118] The Livermore FXD experiment was used to show, for some materials, that crystalline order is preserved through the shock front[113] and to observe a phase transition resulting from shock-compression.[115]

Electron and neutron diffraction techniques would have a similar timing problem although a new pulsed electron diffraction technique[124] produces a shorter, more accurately timed pulse. In the case of electron diffraction, the small range, however, would probably necessitate placing the beam source and target in a vacuum chamber which would be destroyed during each experiment.

In summary, while short wavelength methods may potentially offer desirable information, the difficulty in performing the experiments may at this time far exceed the results which can be obtained.

B. Complementary Techniques

Complementary experiments, even though they may not be performed using dynamic high pressure/temperature systems, can contribute significantly to our understanding of shock-compression phenomenology. We have identified at least three kinds of experiments where static high pressure results can complement dynamic measurements.

1. Structure, Phase and Species Identification. Interpretation of results from shock-compression experiments has frequently been difficult because the behavior and characteristic identifying features, e.g. optical spectra, for many materials are not known at high pressure and temperature. The BSRS experiment described in section A.1.d. is a good example of this lack. Figure 21 depicts the Raman frequency shift measured for shock-compressed benzene. Also, shown is the Raman shift determined under static conditions in a heated diamond anvil cell where the phase of the benzene could be determined visually and by observing the phonon spectra.[87] Only by correlating the BSRS shifts in the dynamic experiments to the results obtained statically where the phase was determined, could we positively identify the shocked benzene as being in the liquid state. Since molecular energy levels and consequently observed spectroscopic features shift significantly during shock-compression, identification of species through and behind the shock front will require similar concomitant experiments.

2. Reaction Phenomenology. An abundance of literature[125-141] exists describing condensed phase energy transfer and relaxation phenomenology at ambient pressures and various temperatures. There is, however, a dearth of studies showing behavior as a result of high pressure effects,[142-145] of large stress gradients, and of temperatures typical in shock-wave environments. Under shock-compression, intra- and inter-molecular forces will change considerably and non-equilibrium conditions may occur. Chemical reactivity and other molecular processes may be dramatically different from that expected based on either extrapolations from ambient conditions or thermodynamic equilibrium. A second kind of complementary experiment is to study energy transfer phenomenology and rates at conditions where molecular energy level shifts and "collision rates," i.e. densities, are comparable to those expected during shock compression. Even though such experiments do not duplicate shock-wave conditions they should provide considerable insight regarding changes in collision-induced transition probabilities and high density many-body effects.

Two experiments are suggested: one which studies the effects of intermolecular forces on collisional vibrational deactivation and a second which looks at changes in vibrational transition probabilities resulting from compressional shifts of molecular vibrational levels. Both experiments use fast pulsed-laser techniques to stimulate and probe the molecular sample. In comparable, actual shock-compression experiments, the stimulating pulse may not be needed if the material translational temperature is sufficiently high.

Ewing et al.[125-130] in a series of experiments using both neat liquid nitrogen and mixtures of liquid nitrogen with small concentrations of additives, measured the vibrational relaxation time of the pure material to be slightly less than 1 min. Figure 22 shows a similar proposed fast pulsed-laser experiment using a high-pressure diamond-anvil cell. The pump beam excites the nitrogen molecule to the first vibrational level using stimulated Raman scattering. The second delayed probe beam measures the population decay of this level via spontaneous anti-Stokes Raman scattering. Presumably, as the pressure in the cell is increased, the relaxation time will decrease.[142-145] At sufficiently high density, the relaxation

rate will be fast enough that if the measurement were made behind a shock-front in a dynamic experiment, substantial population of the excited state in equilibrium with the translational temperature of the shocked material would occur within a few mm of the front. The goal of the experiments is to observe vibrational relaxation in a dense fluid obtained both by shock compression and by a high-pressure cell. In this way one could separate the effects of fluid structure (density) from the effects of intermolecular potentials (temperature).

The second experiment is based on similar psec relaxation experiments of Laubereau et al.[146] and Fendt et al.[147] and ultrasonic studies of Takagi, et al.[135,137] which study the vibrational energy transfer in substituted methanes. The lower vibrational energy levels and some overtone and combination levels in the vicinity of the CH stretch levels near 3000 cm^{-1} are shown in Fig. 23 for dichloromethane, CH_2Cl_2. The results of the studies show that after populating the CH stretch modes using a psec infrared laser pulse (equilibration between the two modes is very rapid) these levels decay through a weak Fermi resonance to an overtone level of the bending modes. The presence of the Fermi resonance is deduced from a line in the infrared spectrum at 2832 cm^{-1} due to the first overtone of the ν_2 bending mode (Fig. 21). ν_1 and ν_6 are the two CH stretching modes and the peak at 2832 cm^{-1} is from $2\nu_2$. We believe that an important aspect of energy transfer during shock compression and shock-compression chemistry is how the energy flows through the vibrational degrees of freedom, i.e., how they are populated from the translational energy of the shock wave[148,149] and if they are in equilibrium. In the case of the above system, compression either using shock-wave techniques or statically using a diamond-anvil cell, will induce a relative shift in the ν_1, ν_6 and ν_2 levels that should change the resonant coupling of the CH fundamental levels and the ν_2 overtone. The relaxation time should change accordingly. Experiments similar to that shown in Fig. 22 using CH_2Cl_2 and other substituted methanes and psec laser spectroscopy can be used to study the intra- or inter-molecular relaxation phenomenology at densities similar to those existing during shock compression. At pressures of several kilobars, the molecules may not exist individually but as some other type of structure with radically shifted energy levels. Interpretation would require a

theoretical approach which differs significantly from the frequently used bimolecular collision model.

3. Unique Features of Shock-Compression. Definitive experiments are needed to elucidate the unique features of shock compression relating to reactivity. Because the phenomena occur extremely rapidly over very small distances and the stress gradients are large, observation of the microscopic behavior is difficult.

Two complementary techniques or, actually, variations of shock-compression experiments, which might provide some insight into behavior in the abrupt shock-front, are suggested. The first is to reduce the strength of the shock wave to a pressure level characteristic of incipient reaction. By doing this, the degree of reactivity may be lessened to that where the region immediately behind the shock-front can be interrogated to reveal evidence of mechanisms in the front itself. The second is to conduct experiments at reduced strain rates using ramp generator or reduced strain rate techniques. By spreading the elusive shock-front region out in space and time to facilitate diagnosis one may be able to observe the effect of large variable stress gradients on molecules and material structures. Both of these methods would be used in conjunction with parallel static experiments.

IV. SUMMARY

Future development of diagnostic techniques for studying the phenomenology of condensed-phase shock-compressed molecular systems will probably evolve as follows. Investigators will continue to use and refine proven methods such as pressure and particle velocity, electrical conductivity and recovery experiments to infer aspects of shock-compression behavior. Some of the more direct measurement techniques, such as Raman scattering, will give specific information about shock-induced reaction, decomposition, phase changes, etc. This information, when used in conjunction with results of established methods, will provide insight into the detailed microscopic phenomenology through and immediately behind the shock front. Complementary high pressure/high temperature static

measurements will be used to test diagnostic tools, determine structure and energy transfer rates at approximate shock-compression conditions and, hopefully help to distinguish between shock and non-shock environments.

Two fundamental limitations for making experimental measurements in the region through and immediately behind shock fronts are the maximum possible spatial resolution which can be achieved and the increased bandwidth of fast temporal measurements. For visible wavelength optical measurements, the diffraction limit, or spatial resolution, is ~1/2 μ. For subpicosecond temporal techniques, the bandwidth, or spectral resolution, is several tens of wavenumbers.

In the near future, say five ye rs, we believe the evolution of diagnostic techniques will enable us to perform the following measurements: (1) determination of vibrational and electronic energy levels for many shock-compressed materials; (2) identification of material phases when shock-compressed; (3) identification for many materials of chemical species resulting from shock-induced decomposition, polymerization, reaction, etc.; (4) determination of reaction-rate phenomenology for shock-compressed materials, i.e., how do rates and phenomenology change with large compressions and high temperatures?; and (5) measurement of some details of shock-front structure possibly providing insight regarding the unique features of the shock process. When the results of these measurements are coupled with presently known information, the possibilities for increasing our phenomenological understanding of the shock-compression process are numerous.

The authors wish to thank C. W. Caldwell for his assistance in performing the shock-w experiments and Mary Ann Lucero for typing the manuscript.

V. REFERENCES

1. C. A. Forest, "Burning and Detonation," LA-7245, (Los Alamos National Laboratory Report, Los Alamos, New Mexico 1978).

2. C. L. Mader, Numerical Modeling of Detonation, (University of California Press, Berkeley, California 1979).

3. E. L. Lee and C. M. Tarver, Phys. Fluids 23, 2362 (1980).

4. J. Wackerle, R. L. Rabie, M. J. Ginsberg and A. B. Anderson in Proceedings of the Symposium on High Dynamic Pressures, (Commissariat á l'Energie Atomique, Paris, France 1978) p. 127.

5. M. Cowperthwaite in Proceedings of the Symposium on High Dynamic Pressures, (Commissariat á l'Energie Atomique, Paris, France 1978) p. 201.

6. J. W. Nunizato in Shock Waves in Condensed Matter - 1983, American Physical Society Topical Conference, Santa Fe, New Mexico 1983.

7. J. W. Nunizato and E. K. Walsh, Arch. Rational Mech. Anal. 73, 285 (1980).

8. J. N. Johnson, private communication.

9. W. C. Davis in Proc. 7th Symp. Detonation, (Annapolis, Maryland 1981), p. 531.

10. M. J. Beran, Statistical Continuum Theories, (Interscience Publishers, New York 1968).

11. D. Stroud, Phys. Rev. B 12, 3368 (1975).

12. D. Stroud and F. P. Pan, Phys. Rev. B 17, 1602 (1978).

13. W. Lamb, D. M. Wood and N. W. Ashcroft, Phys. Rev. B 21, 2248 (1980).

14. J. E. Gubernatis and J. A. Krumhansl, J. Appl. Phys. 46, 1875 (1975).

15. J. E. Gubernatis in Conference on Electrical Transport and Optical Properties of Inhomogeneous Media, (The Ohio State University, Columbus, Ohio 1977).

16. J. E. Gubernatis and E. Domany, Submitted to Wave Motion.

17. E. Kröner, J. Phys. F.: Metal Phys. 8, 2261 (1978).

18. J. K. Dienes in Proceedings of the Colloque International du CNRS n°351 Failure Criteria of Structured Media, (Villard-de-Lans, France 1983).

19. A. Delpuech and A. Menil in Shock Waves in Condensed Matter - 1983, American Physical Society Topical Conference, Santa Fe, New Mexico 1983.

20. S. B. Kormer, Sov. Phys.-Uspekhi 11, 229 (1968).

21. A. N. Dremin and V. Yu. Klimenko, "On the Role of the Shock Wave Front in Organic Substances Decomposition," Gas Dynamics of Explosions and Reactive Systems, Minsk, USSR 1981.

22. A. W. Campbell, W. C. Davis and J. R. Travis, Phys. Fluids 4, 498 (1961).

23. P. A. Persson and T. Sjölin in Proc. 5th Symp. Detonation, (Pasadena, California 1970, ACR-184), p. 153.

24. S. Poulard, C. Kassel, R. Fiat and B. Linares in Proc. Symp. Expl. and Pyrotech. 8th, (Los Angeles, California 1974).

25. P. A. Urtiew and R. Grover, J. Appl. Phys. 48, 112 (1977).

26. G. A. Lyzenga in Shock Waves in Condensed Matter - 1981, Am. Inst. Phys. Proc. 78, edited by W. S. Nellis, L. Seaman and R. A. Graham, (New York 1982), p. 268.

27. K. Kondo, T. J. Ahrens and A. Sawaoka in Shock Waves in Condensed Matter - 1981, Am Inst. Phys. Proc. 78, edited by W. S. Nellis, L. Seaman and R. A. Graham, (New York 1982), p. 299.

28. D. R. Schmitt and T. J. Ahrens in Shock Waves in Condensed Matter - 1983, American Physical Society Topical Conference, Santa Fe, New Mexico 1983.

29. M. B. Boslough, T. J. Ahrens, A. C. Mitchell and W. J. Nellis, in Shock Waves in Condensed Matter - 1983, American Physical Society Topical Conference, Santa, New Mexico 1983.

30. W. G. VonHolle and J. J. Trimble in Proc. 6th Symp. Detonation, (Coronado, California 1976), ACR-221, p. 691.

31. W. G. VonHolle in Fast Reactions in Energetic Systems, edited by C. Capellos and R. F. Walker (D. Reidel, Dorecrecht, Holland 1981).

32. W. G. VonHolle and C. M. Tarver in Proc. 7th Symp. Detonation, (Annapolis, Maryland 1981), p. 531.

33. W. G. VonHolle in Shock Waves in Condensed Matter - 1983, American Physical Society Topical Conference, Santa Fe, New Mexico 1983.

34. R. G. McQueen, J. N. Fritz and J. W. Hopson in preparation for publication.

35. P. J. Brannon, C. H. Konrad, R. W. Morris, E. D. Jones, J. R. Asay, "Spectral and Spatial Studies of Shock-Induced Luminescence from

Quartz," SAND-82-2469, (Sandia National Laboratories, Albuquerque, New Mexico 1983).

36. P. J. Brannon, R. W. Morris, C. H. Konrad and J. R. Asay in Shock Waves in Condensed Matter - 1983, American Physical Society Topical Conference, Santa Fe, New Mexico 1983.

37. C. Schulz, B. Linares, J. Cherville and S. Poulard in Proc. Symp. Expl. and Pyrotech. 8th, (Los Angeles, California 1974), AD-789, p. 49.

38. L. R. Dosser and J. H. Mohler, "Emission Spectroscopy of Energetic Materials," 74th Meeting of JOWOG-9, Los Alamos National Laboratory, Los Alamos, New Mexico 1981.

39. L. R. Dosser and J. H. Mohler, "Time-Resolved Emission Spectroscopy of Energetic Materials," Monsanto Research Corporation - Mound Facility (Miamisburg, Ohio) Quarterly Progress Report, October-December, 1982.

40. L. Davison and R. A. Graham, Phys. Reports 55, 255 (1979).

41. S. S. Penner, Quantitative Molecular Spectroscopy and Gas Emissivities, (Addison-Wesley, Reading, Massachusetts 1959).

42. R. M. Goody, Atmospheric Radiation I, (Oxford University Press, London 1964).

43. J. M. Walsh and M. H. Rice, J. Chem. Phys. 26, 815 (1957).

44. H. G. David and A. H. Ewald, Austr. J. Appl. Sci. 11, 317 (1960).

45. A. H. Ewald in High Pressure in Science and Technology, IX AIRAPT Conference, Albany, New York 1983.

46. O. B. Yakusheva, V. V. Yakushev and A. N. Dremin, Sov. Phys. Doklady 14, 1189 (1970).

47. O. B. Yakusheva, V. V. Yakushev and A. N. Dremin, High Temp.-High Pres. 3, 261 (1971).

48. O. B. Yakusheva, V. V. Yakushev and A. N. Dremin, Russ. Jour. Phys. Chem. 51, 973 (1977)

49. E. S. Gaffney and T. J. Ahrens, Jour. Geo. Res. 78, 5942 (1973).

50. Ya. B. Zel'dovich, S. B. Kormer, M. V. Sinitsyn and K. B. Yushko, Sov. Phys. Doklady 6, 494 (1961).

51. T. J. Ahrens and M. H. Ruderman, J. Appl. Phys. 37, 4758 (1966).

52. C. F. Petersen and J. T. Rosenberg, J. Appl. Phys. 40, 3044 (1969).

53. H. S. Yadav, D. S. Murty, S. N. Verma, K. H. C. Sinha, B. M. Gupta and D. Chand, J. Appl. Phys. 44, 2179 (1973).

54. D. R. Hardesty, J. Appl. Phys. 47, 1994 (1976).

55. T. Goto, G. R. Roseman and T. J. Ahrens in High-Pressure Science and Technology, Vol. 2, Sixth AIRAPT Conference, edited by M. S. Barber and K. D. Timmerhaus , (Plenum Press, New York 1979), p. 895.

56. T. Goto, T. J. Ahrens, G. R. Rossman and Y. Syono, Phys. Earth Planet. Int. 22, 277 (1980).

57. G. E. Duvall, K. M. Ogilvie, R. Wilson, P. M. Bellamy and P. S. P. Wei, Nature 296, 846 (1982).

58. R. S. Hixson, P. M. Bellamy, G. E. Duvall and C. R. Wilson in Shock Waves in Condensed Matter - 1981, Am. Inst. Phys. Proc. 78,

edited by W. S. Nellis, L. Seaman and R. A. Graham, (New York 1981), p. 282.

59. K. M. Ogilvie and G. E. Duvall, J. Chem. Phys. 78, 1077 (1983).

60. R. H. Granholm, G. E. Duvall and P. M. Bellamy in Shock Waves in Condensed Matter - 1983, American Physical Society Topical Conference, Santa Fe, New Mexico 1983.

61. G. E. Duvall, R. H. Granholm and P. M. Bellamy in Shock Waves in Condensed Matter - 1983, American Physical Society Topical Conference, Santa Fe, New Mexico 1983.

62. D. S. Bethune, J. R. Lankard, M. M. T. Loy and P. P. Sorokin, IBM J. Res. Develop. 23, 556 (1979).

63. Ph. Avouris, D. S. Bethune, J. R. Lankard, J. A. Ors and P. P. Sorokin, J. Chem. Phys. 74, 2304 (1981).

64. A. J. Schell-Sorokin, D. S. Bethune, J. R. Lankard, M. M. T. Loy and P. P. Sorokin, J. Phys. Chem 86, 4653 (1982).

65. F. W. Neilson, W. B. Benedick, W. P. Brooks, R. A. Graham and G. W. Anderson in Les Ondes Detonation (Editions du Centre National de la Recherche Scientifique, Paris 1962), p. 391.

66. W. P. Brooks, J. Appl. Phys. 36, 2788 (1965).

67. R. K. Linde and D. G. Doran, Nature 212, 27 (1966).

68. R. A. Graham and W. J. Halpin, J. Appl. Phys. 39, 5077 (1968).

69. J. H. Blackburn and L. B. Seely, Nature 194, 370 (1962).

70. J. H. Blackburn and L. B. Seely, Nature 202, 276 (1964).

71. S. Paterson, Nature 203 1057 (1964).

72. A. S. Eckbreth, P. A. Bonczyk and J. F. Verdieck, App. Spectrosc. Rev. 13, 15 (1977).

73. J. C. Wright, Appl. Spectrosc. 34, 151 (1980).

74. H. G. Drickamer, Ann. Rev. Phys. Chem. 33, 25 (1982).

75. F. Boisard, C. Tombini and A. Menil in Proc. 7th Symp. Detonation, (Annapolis, Maryland 1981), p. 531.

76. A. Delpuech, J. Cherville and C. Michaud in Proc. 7th Symp. Detonation, (Annapolis, Maryland 1981), p. 36.

77. M. H. Tailleur and J. Cherville, Propellants, Expl. and Pyrotech. 7, 22 (1982).

78. N. Holmes in Shock Waves in Condensed Matter - 1983, American Physical Society Topical Conference, Santa Fe, New Mexico 1983.

79. D. L. Rousseau, J. M. Friedmand and P. F. Williams in Raman Spectroscopy of Gases and Liquids, edited by A. Weber (Springer-Verlag, Berlin 1979), p. 203.

80. W. H. Woodruff and S. Farquharson in New Applications of Lasers to Chemistry (American Chemical Society Symposium Series 85), edited by G. M. Hieftje (American Chemical Society, Washington, DC 1978), p. 215.

81. R. F. Dallinger, S. Farquharson, W. H. Woodruff and M. A. J. Rodgers, Am. Chem. Soc. 103, 7433 (1981).

82. S. C. Schmidt, D. S. Moore, D. Schiferl and J. W. Shaner, Phys. Rev. Lett. 50, 661 (1983).

83. M. Maier, W. Kaiser and J. A. Giordmaine, Phys. Rev. 177, 580 (1969).

84. D. V. J. Linde, M. Maier and W. Kaiser, Phys. Rev. 178, 178 (1969).

85. M. H. Rice, R. G. McQueen and J. M. Walsh, Solid State Physics 6, (Academic Press, New York 1958), 1.

86. R. D. Dick, J. Chem. Phys. 57, 6021 (1970).

87. W. D. Ellenson and M. Nicol, J. Chem. Phys. 61, 1380 (1974), this mode is called ν_2 in G. Herzberg, Infrared and Raman Spectra, (Van Nostrand Reinhold, New York 1968).

88. R. N. Keeler, G. H. Bloom and A. C. Mitchell, Phys. Rev. Lett. 17, 852 (1966).

89. A. N. Dremin and L. V. Barbare in Shock Waves in Condensed Matter - 1981, Am. Inst. Phys. Proc. 78, edited by W. S. Nellis, L. Seaman and R. A. Graham, (New York 1981) p. 270.

90. W. J. Jones and B. P. Scoicheff, Phys. Rev. Lett. 13, 657 (1964).

91. E. S. Yeung in New Applications of Lasers to Chemistry (American Chemical Society Symposium Series 85, edited by G. M. Heiftje (American Chemical Society, Washington, DC 1973), p. 193.

92. W. G. VonHolle and R. A. McWilliams in Laser Probes for Combustion Chemistry (American Chemical Society Symposium Series 134), edited by D. R. Crosley (American Chemical Society, Washington, DC 1983), p. 319.

93. P. D. Maker and R. W. Terhune, Phys. Rev. 137, A801 (1965).

94. W. M. Tolles, J. W. Nibler, J. R. McDonald and A. B. Harvey, Appl. Spectrosc. 31, 253 (1977).

95. D. S. Moore, S. C. Schmidt and J. W. Shaner, Phys. Rev. Lett. 50, 1819 (1983).

96. W. B. Roh, P. W. Schreiber and J. P. E. Taran, Appl. Phys. Lett. 29, 174 (1976).

97. J. J. Valentini, D. S. Moore and D. S. Bomse, Chem. Phys. Lett. 83, 217 (1981).

98. A. C. Eckbreth, Appl. Phys. Lett. 32, 421 (1978).

99. D. Heiman, R. W. Hellworth, M. D. Levenson and G. Martin, Phys. Rev. Lett. 36, 189 (1976).

100. D. S. Moore, S. C. Schmidt, D. Schiferl and J. W. Shaner in High Pressure in Science and Technology, IX AIRAPT Conference, Albany, New York 1983.

101. S. C. Schmidt, D. S. Moore and J. W. Shaner in Shock Waves in Condensed Matter - 1983, American Physical Society Topical Conference, Santa Fe, New Mexico 1983.

102. R. Y. Chiao, C. H. Townes and B. P. Stoicheff, Phys. Rev. Lett. 12, 592 (1964).

103. E. Garmire and C. H. Townes, Appl. Phys. Lett. 5, 84 (1964).

104. M. Maier, Phys. Rev. 166, 113 (1968).

105. G. H. Bloom and R. N. Keeler, J. Appl. Phys. 45, 1200 (1974).

106. Ya. B. Zel'dovich, S. B. Kormer, M. V. Sinitsyn and K. B. Yushko, Sov. Phys. Doklady 6, 494 (1961).

107. P. Harris, J. Chem. Phys. 74, 6864 (1981).

108. P. Harris and H. N. Presles in Shock Waves in Condensed Matter - 1983, American Physical Society Topical Conference, Santa Fe, New Mexico 1983.

109. Y. B. Zel'dovich, S. B. Kormer, G. V. Krishkevich and K. B. Yushko, Sov. Phys. Doklady 11, 936 (1967).

110. R. A. Graham in Shock Waves in Condensed Matter - 1981, Am. Inst. Phys. Proc. 78, edited by W. S. Nellis, L. Seaman and R. A. Graham, (New York 1981), p. 52.

111. Q. Johnson, R. N. Keeler and J. W. Lyle, Nature 213, 1114 (1967).

112. Q. Johnson, A. Mitchell, R. N. Keeler and L. Evans, Phys. Rev. Lett. 25, 1099 (1970).

113. Q. Johnson, A. Mitchell and L. Evans, Nature 231, 310 (1971).

114. Q. Johnson, A. C. Mitchell and L. Evans, Appl. Phys. Lett. 21, 29 (1972).

115. Q. Johnson and A. C. Mitchell, Phys. Rev. Lett. 29, 1369 (1972).

116. F. Jamet, Comptes Rend. Acad. Sci. (Paris) 271, 714 (1970).

117. L. A. Egorov, E. V. Nitochkina and Yu. K. Orekin, JETP Lett. 16, 4 (1972).

118. K. Kondo, T. Mashimo, A. Sawaoka and S. Saito in High-Pressure Science and Technology Vol. 2, Sixth AIRAPT Conference, edited by K. D. Timmerhaus and M. S. Barber, (Plenum Press, New York 1979), p. 883.

119. F. Jamet and G. Thomer, Comptes Rend. Acad. Sci. (Paris) 179, 501 (1974).

120. R. E. Green, Jr., Rev. Sci. Instr. 46, 1257 (1975).

121. Q. Johnson, A. Mitchell and L. Evans, Rev. Sci. Instrum. 42, 999 (1971).

122. A. C. Mitchell, Q. Johnson and L. Evans, Rev. Sci. Instrum. 44, 497 (1973).

123. A. Sawaoka, private communication.

124. B. M. Schwarzschild, Phys. Today 36, No. 2, 17 (1983).

125. W. F. Calaway and G. E. Ewing, Chem. Phys. Lett. 30, 485 (1975).

126. W. F. Calaway and G. E. Ewing, J. Chem. Phys. 63, 2842 (1975).

127. C. Manzanares and G. E. Ewing, J. Chem. Phys. 69, 1418 (1978).

128. C. Manzanares and G. E. Ewing, J. Chem. Phys. 69, 2803 (1978).

129. D. W. Chandler and G. E. Ewing, J. Chem. Phys. 73, 4904 (1980).

130. D. W. Chandler and G. E. Ewing, J. Phys. Chem. 85, 1994 (1981).

131. W. Kaiser and A. Laubereau in Nonlinear Spectroscopy (Proc. International School of Physics "Enrico Fermi," Course LXIV), edited by N. Bloembergen (North-Holland Publishing Co., Amsterdam 1977), p. 404.

132. A. Laubereau and W. Kaiser, Rev. Mod. Phys. 50, 607 (1978).

133. D. Samios and Th. Dorfmüller, Mol. Phys. 41, 637 (1980).

134. Th. Dorfmüller and D. Samios, Mo. Phys. 43, 23 (1981).

135. K. Takagi, P.-K. Choi and K. Negishi, J. Acoust. Soc. Am. 62, 354 (1977).

136. K. Takagi and K. Negishi, J. Chem. Phys. 72, 1809 (1980).

137. K. Takagi, P.-K. Choi and K. Negishi, J. Chem. Phys. 74, 1424 (1982).

138. P.-K. Choi, K. Takagi and K. Negishi, J. Chem. Phys. 74, 1438 (1981).

139. J. T. Yardley, Introduction to Molecular Energy Transfer, (Academic Press, New York 1980).

140. C. Capellos and R. F. Walker, Fast Reactions in Energetic Systems, (D. Reidel Publishing Co., Dordrecht, Holland 1980).

141. P. M. Rentzepis, Science 218, 1183 (1982).

142. M. Chatelet, G. Widenlocher and B. Oksengorn in High Pressure Science and Technlogy, Vol. 2, edited by B. Vodar and Ph. Marteau, (Pergamon Press, Oxford 1979), p. 628.

143. M. Chatelet, B. Oksengorn, G. Widenlocher and Ph. Marteau, J. Chem. Phys. 75, 2374 (1981).

144. M. Chatelet, Abstract for Regional AIRAPT Meeting, Van Der Walls Laboratory, University of Amsterdam, The Netherlands, June 21-22, 1982.

145. M. Chatelet, J. Kieffer and B. Oksengorn, to be published Chem. Phys.

146. A. Laubereau, S. F. Fisher, K. Spanner and W. Kaiser, Chem. Phys. 31, 335 (1978).

147. A. Fendt, S. F. Fischer and W. Kaiser, Chem. Phys. 57, 55 (1981).

148. D. J. Pastine, D. J. Edwards, H. D. Jones, C. T. Richmond and K. Kim in High-Pressure Science and Technology Vol. 2, Sixth AIRAPT Conference, edited by K. D. Timmerhaus and M. S. Barber, (Plenum Press, New York 1979), p. 364.

149. F. J. Zerilli in Shock Waves in Condensed Matter - 1983, American Physical Society Topical Conference, Santa Fe, New Mexico 1983.

TABLE I. EMISSION/ABSORPTION/FLUORESCENCE SPECTROSCOPY

Technique	Difficulties	Advantages
Emission	Emission occurs along an optical path.	Radiation measurement can give estimate of temperature.
	Difficult in infrared because of lack of detector time resolution.	Emission lines can give some indication of species.
	Emission lines appear against a bright background.	
Absorption	Absorption occurs along an optical path.	Absorption band shifts can give estimate of structure changes.
	Difficult in infrared because of lack of detector time resolution and bright emission background.	Absorption bands can give some indication of species.
	Absorption occurs from complicated vibronic states making interpretation difficult.	
	Absorption could appear as a small signal against large background.	

TABLE I. Continued

Technique	Difficulties	Advantages
Infrared Absorption Using Parametric Conversion	Absorption occurs along an optical path.	Absorption band shifts can give estimate of structure changes.
	May be hard to implement.	Good temporal resolution
	Absorption could appear as a small signal against large background.	Improved detection sensitivity in infrared.
Fluorescence	Difficult to interpret because of many variables.	Fluorescence can give some indication of species.
	Signal could appear against a bright background.	Can measure intra-level conversion rates.
		Can achieve some spatial resolution.
		Enough intensity for psec time resolution.

TABLE II. RAMAN SPECTROSCOPY

Technique	Temporal Resolution (ns)	Spatial Resolution (μ)	Difficulties	Advantages
Incoherent				
Spontaneous	10	10	Low sensitivity limits temporal and spatial resolution.	Can identify vibrational spectra and species.
			Difficult in high emission background applications.	Can measure temperature.
			Difficult where fluorescence or photochemistry occurs.	
Resonance	10^{-4}–10^{-4}	10	May require small species concentrations.	Can identify vibrational spectra and species.
			Could have competing fluorescence effects.	Increased sensitivity compared to spontaneous Raman scattering.
Coherent				
Stimulated	10^{-4}–1	2000	Spatial resolution marginal.	Can identify single vibrational spectra.
			High power levels required.	Good temporal resolution.
			Limited detection capability (single mode and species).	Scattered beam comes back along incident beam.

Technique	Temporal Resolution (ns)	Spatial Resolution (μ)	Difficulties	Advantages
Inverse	10^{-4}–10	10	Appears as a small signal on large background.	Can identify vibrational spectra and species. Does not require phase matching. Good spatial resolution. Good temporal resolution. All Raman active molecules and modes scatter. No non-resonant background.
Anti-Stokes, Stokes (CARS, CSRS) [BOXCARS]	10^{-4}–10	1000 [100]	Phase matching required.	Can identify vibrational spectra and species. Spatial resolution adequate. Good temporal resolution. Good detection sensitivity. All Raman active molecules and modes scatter.
Raman Induced Kerr Effect (RIKES)	10^{-4}–10	10	Sensitive to birefringence effects.	Can identify vibrational spectra and species. Does not require phase matching. Good spatial resolution. Good temporal resolution. All Raman active molecules and modes scatter.
Other			Complicated.	

VI. FIGURE CAPTIONS

Figure 1. Conceptual Description for Modeling Shock-Wave Propagation in Heterogeneous Materials.

Figure 2. Refractive Effects of Shock Wave on Optical Beam.

Figure 3. Detonation Wave Microstructure for Nitromethane and a Nitromethane/Acetone Mixture.[9]

Figure 4. Cool Layer Opacity Effects on Emission Spectrum.

Figure 5. Proposed Time Resolved Emission Experiment.

Figure 6. Shock-Compression Absorption Spectroscopy Experiments.[57].

Figure 7. Time-Resolved Infrared Spectral Photography Experiment.[62]

Figure 8. Vibronic State Single Photon Fluorescence.

Figure 9. Molecular Vibration Raman Scattering.

Figure 10. Spontaneous Raman Scattering Experiments.[19,75-77]

Figure 11. Coherent Raman Scattering Techniques.

Figure 12. Backward Stimulated Raman Scattering Experiment.[82]

Figure 13. Scattered Light Spectrogram for Shock-Compressed Benzene.[82]

Figure 14. Benzene Ring-Stretching Mode Vibrational Frequency Shifts (With Respect to 992 cm^{-1}) Versus Pressure,[82] Data Recorded Using BSRS and RBBCARS Are Denoted by Circles and Triangles Respectively. The Single Triangle for RBBCARS Represents Two Data Points. Uncertainties in the Data Are Given on One Data Point.

Figure 15. Proposed Inverse Raman and Raman Induced Kerr Effect Scattering Experiments.[33,92]

Figure 16. Reflected Broadband Coherent Anti-Stokes Raman Scattering Experiment.[95]

Figure 17. RBBCARS Spectra.[95] The Ambient Peak Positions of the Two Species Are 992 cm^{-1} for Benzene and 945 cm^{-1} for Benzene $-d_6$.

Figure 18. Raman Induced Kerr Effect Scattering Experiment.[100,101]

Figure 19. RIKES Spectra of Two Shock-Compressed and One Ambient Pressure Benzene Experiments.[100,101] The Position of the Ambient Unshifted Vibrational Frequency at 992 cm^{-1} Is Given by the Lower Trace. The Krypton Calibration Lines Are 5570.289Å and 5562.225Å.

Figure 20. Shock-Compression, Flash X-Ray Diffraction Experiments.[112]

Figure 21. Benzene Ring Stretching Vibrational Mode Frequency Shift Versus Pressure and Temperature.[82]

Figure 22. Pressure Dependent Vibrational Relaxation Time Experiment. The $LiNbO_3$ Cells are for Generating Infrared Pulses for Populating Non-Raman Active Levels in Molecules Other Than Nitrogen.

Figure 23. Vibrational Energy Levels, Some Overtones and Combinations and Infrared Spectrum: CH_2Cl_2.[132,137]

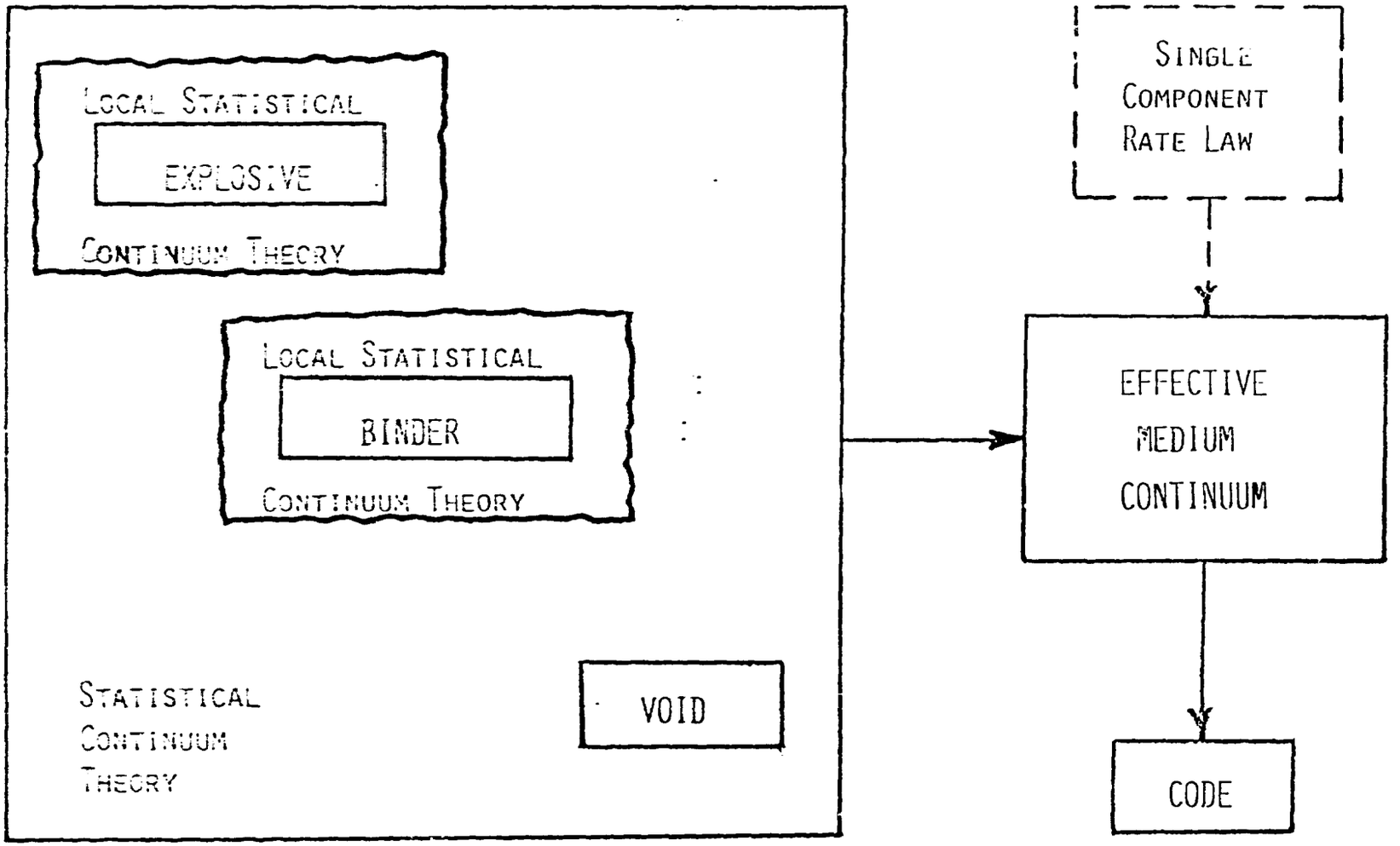
LOCAL STATISTICAL
EXPLOSIVE
CONTINUUM THEORY
LOCAL STATISTICAL
BINDER
CONTINUUM THEORY
STATISTICAL
CONTINUUM
THEORY
VOID
SINGLE
COMPONENT
RATE LAW
EFFECTIVE
MEDIUM
CONTINUUM
CODE

Figure 1.

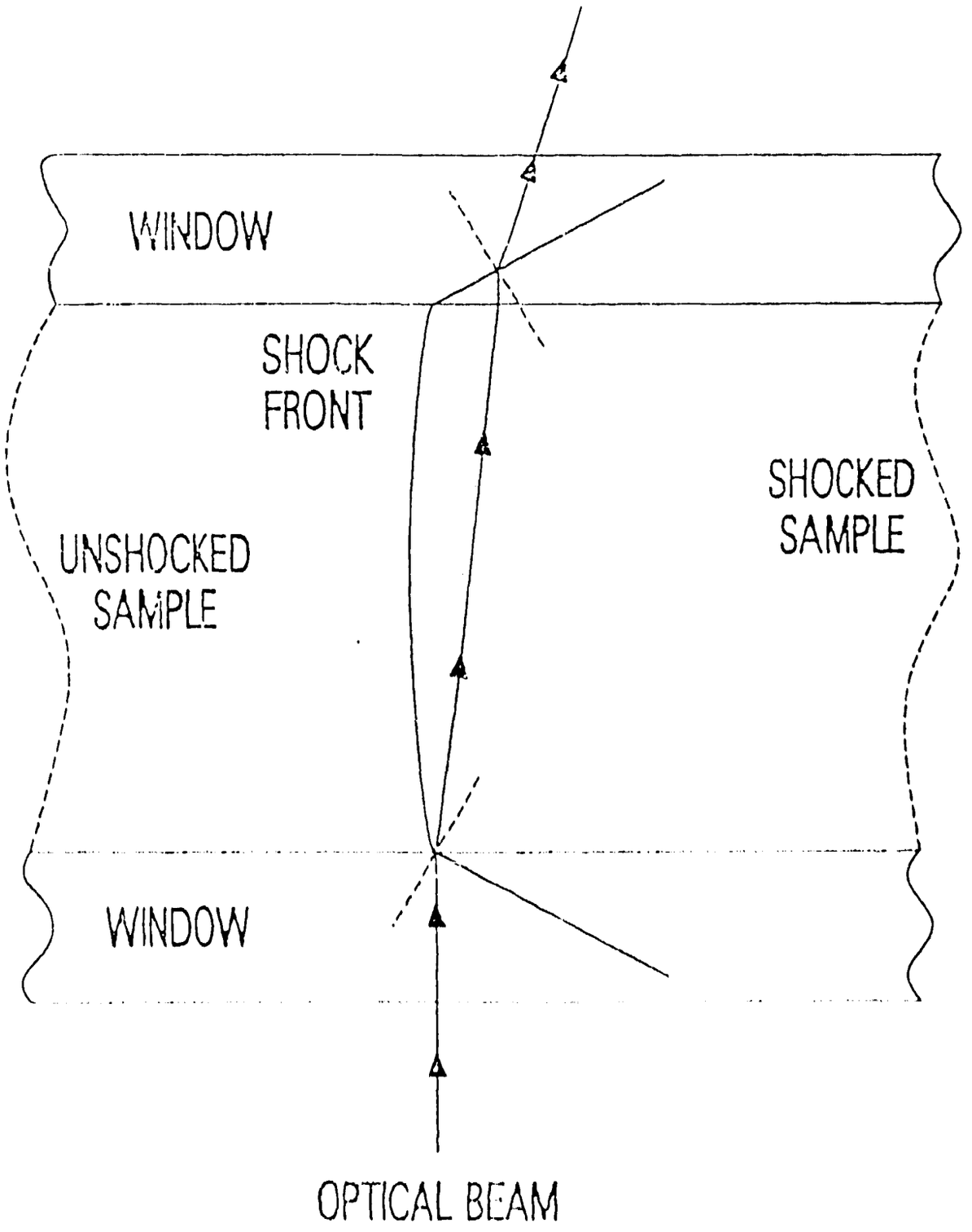
WINDOW
SHOCK
FRONT
SHOCKED
SAMPLE
UNSHOCKED
SAMPLE
WINDOW
OPTICAL BEAM

Figure 2.

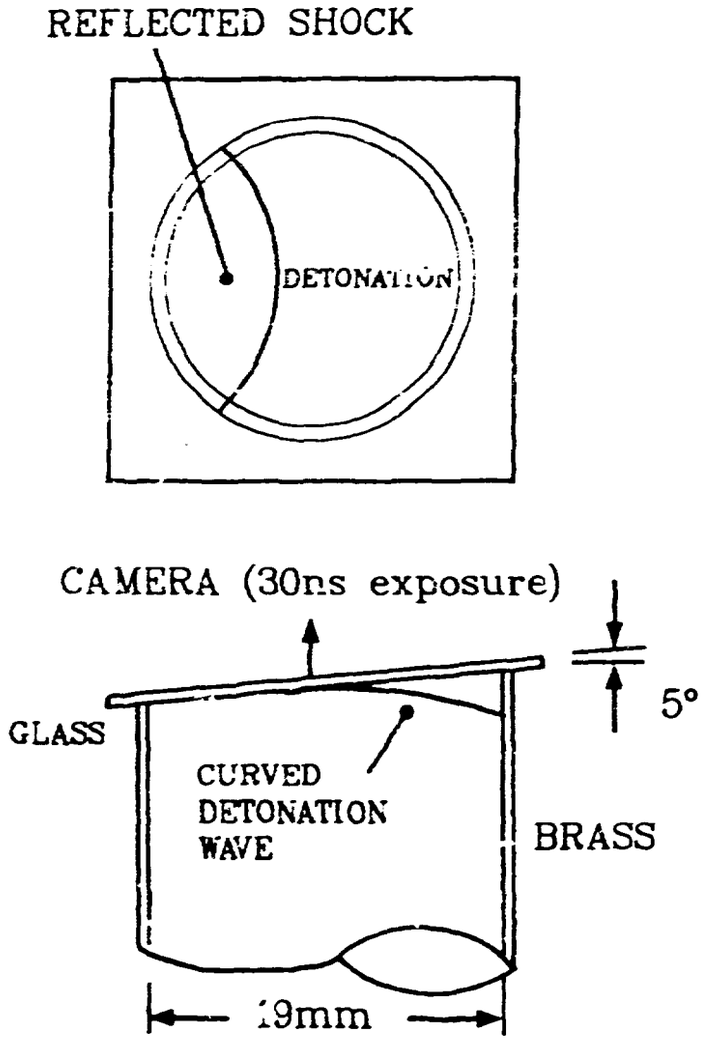

FROM DAVIS

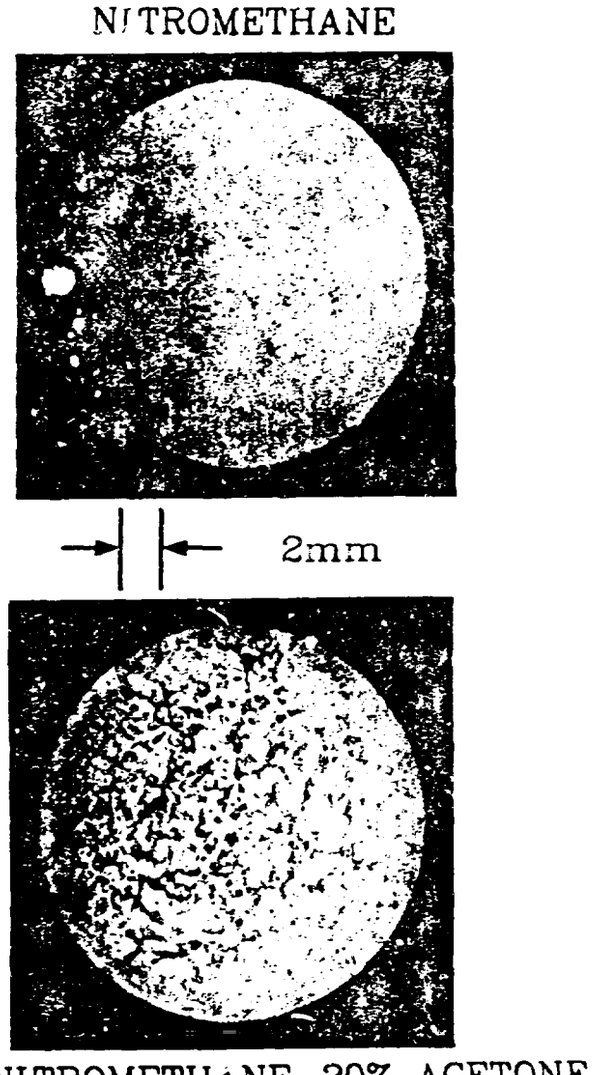

80% NITROMETHANE, 20% ACETONE

Figure 3.

EFFECTS OF OPACITY

RADIATIVE TRANSFER EQUATION FOR LAYER:

$$R_\lambda = \epsilon_\lambda R^0_\lambda + (1 - \epsilon_\lambda) R'_\lambda$$

R_λ – RADIATION LEAVING LAYER

R'_λ – RADIATION ENTERING LAYER

R^0_λ – BLACKBODY RADIATION OF LAYER

ϵ_λ – EMISSIVITY OF LAYER

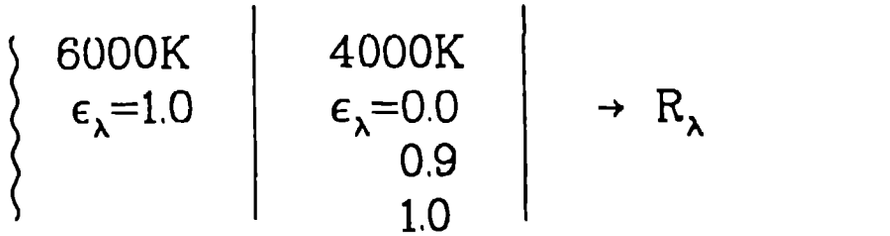

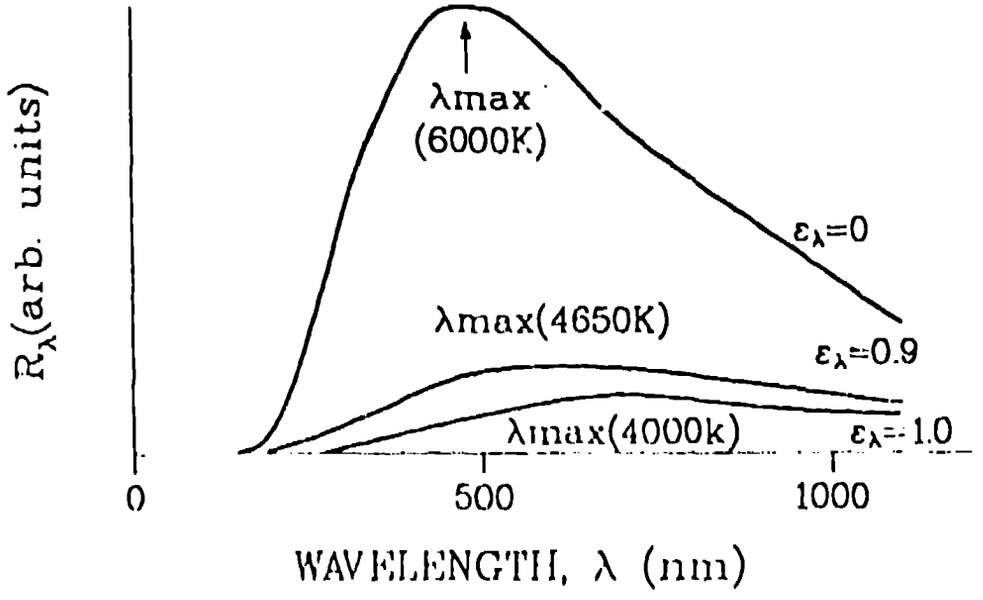

Figure 4.

TIME RESOLVED EMISSION SPECTROSCOPY

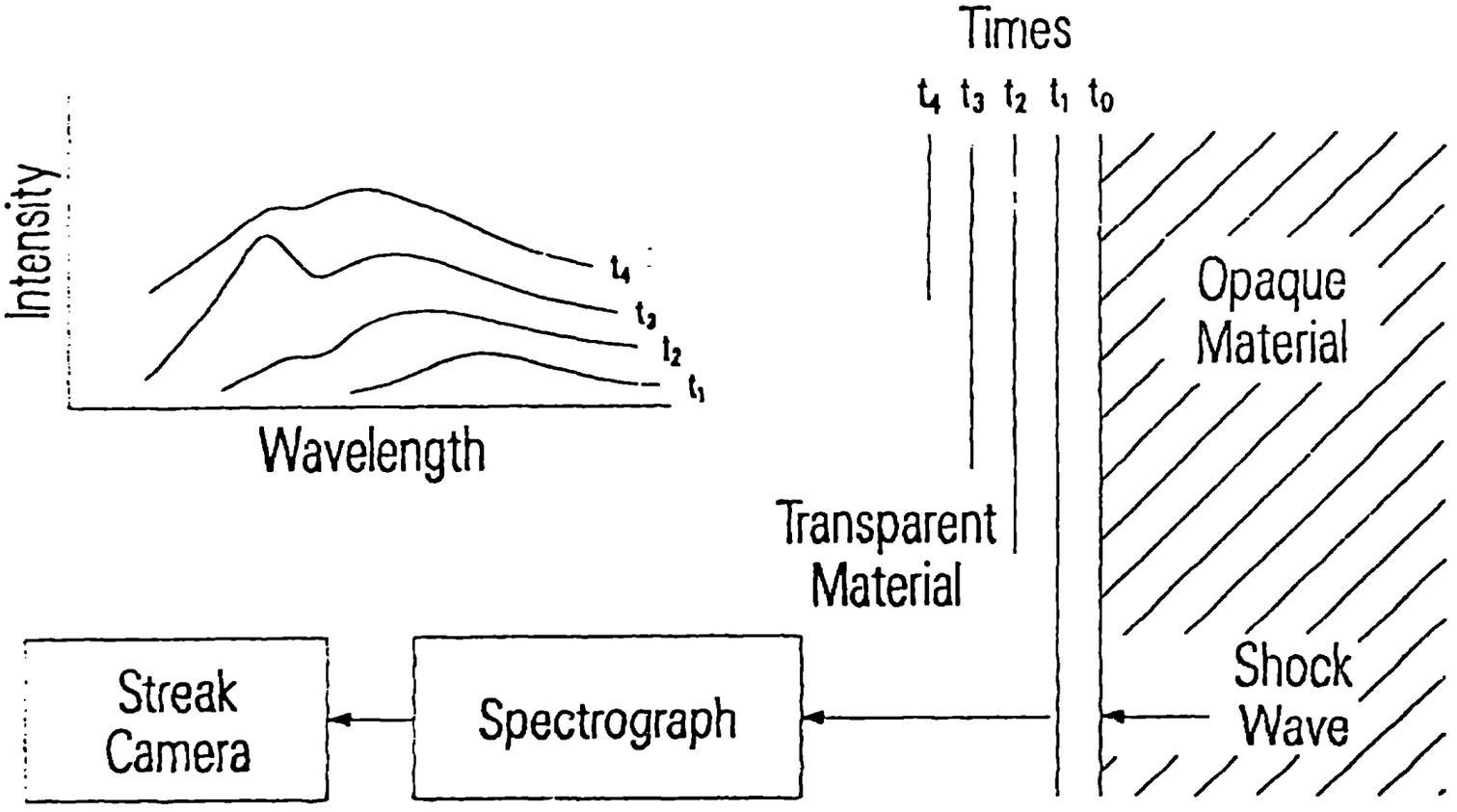

Figure 5.

ABSORPTION SPECTROSCOPY

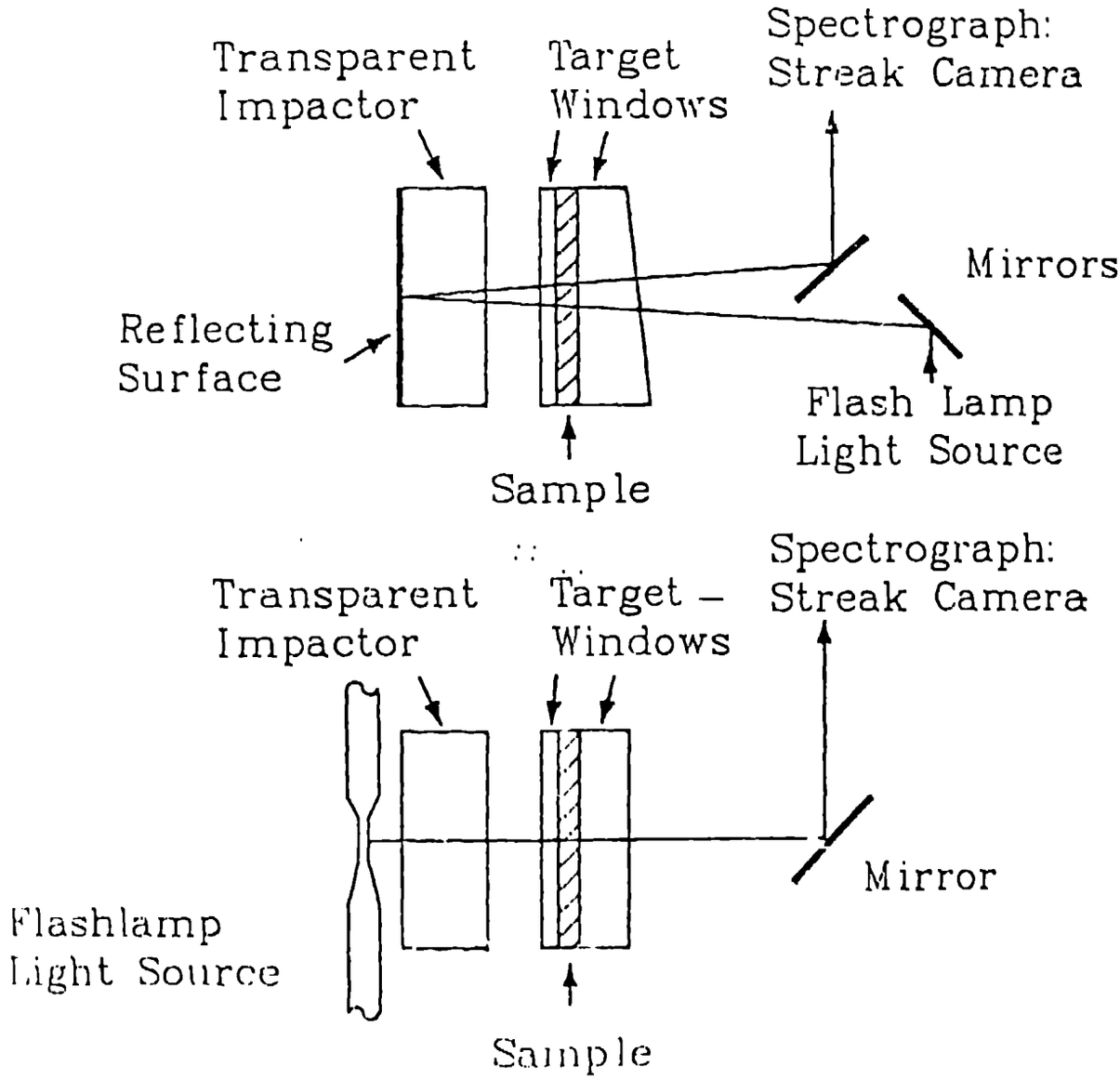

FROM DUVALL, OGILVIE, WILSON, BELLAMY AND WEI

Figure 6.

TIME RESOLVED INFRARED SPECTRAL PHOTOGRAPHY

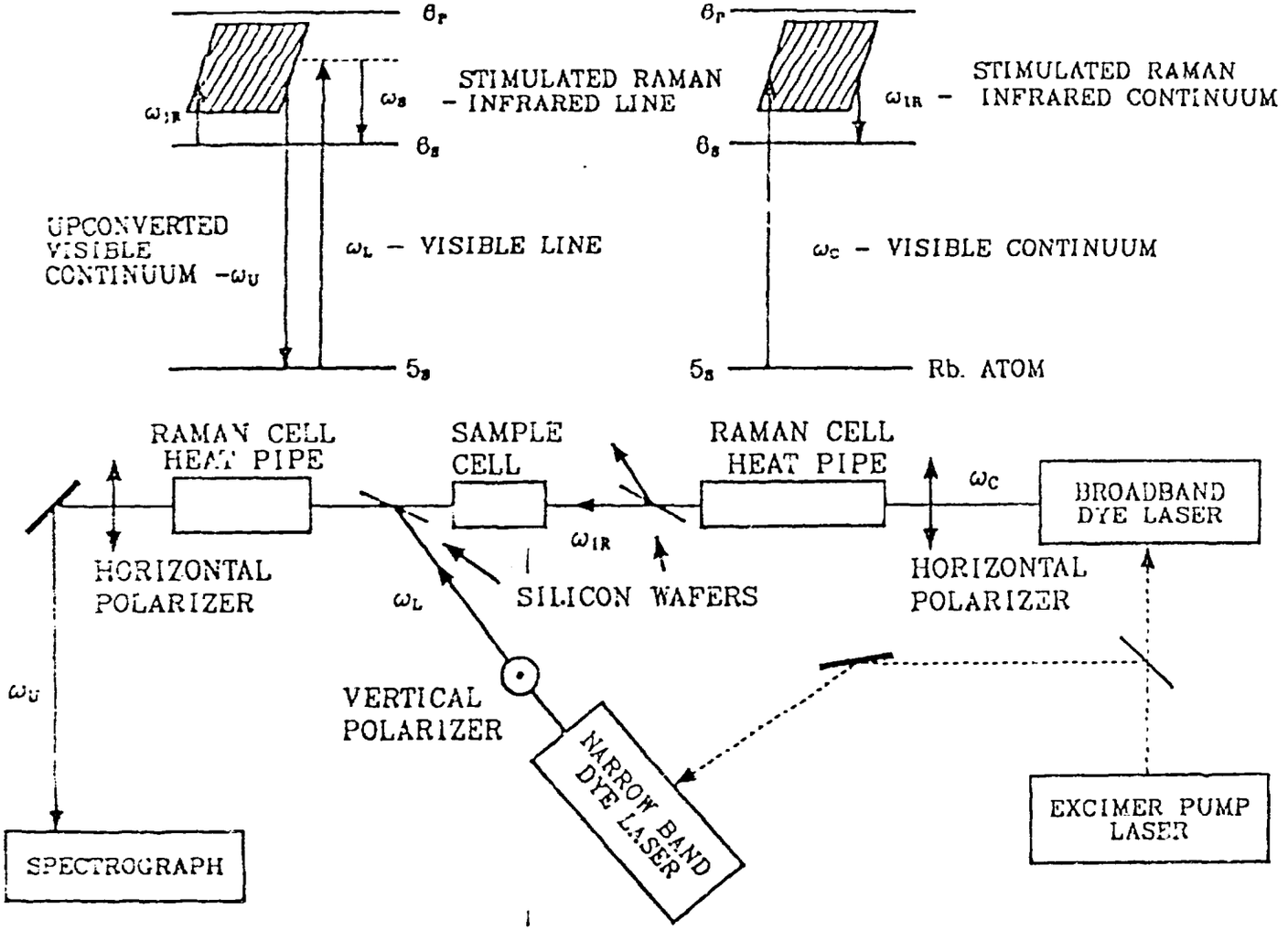

FROM BETHUNE, LANKARD, LOY AND SOROKIN

Figure 7.

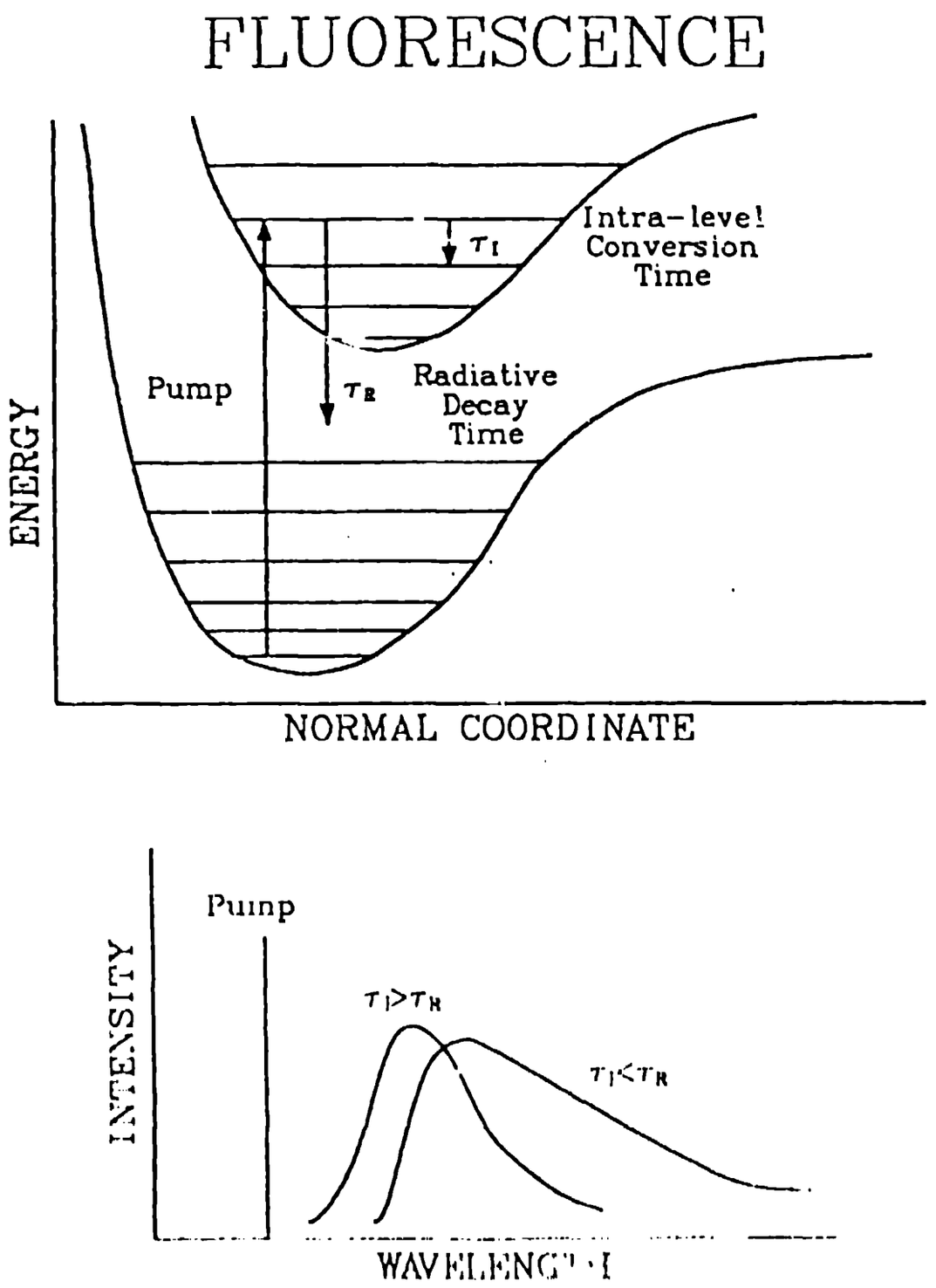
FLUORESCENCE
Intra-level Conversion Time
τ_I
Pump
τ_R
Radiative Decay Time
ENERGY
NORMAL COORDINATE
Pump
$\tau_I > \tau_R$
$\tau_I < \tau_R$
INTENSITY
WAVELENGTH

Figure 3.

RAMAN SCATTERING

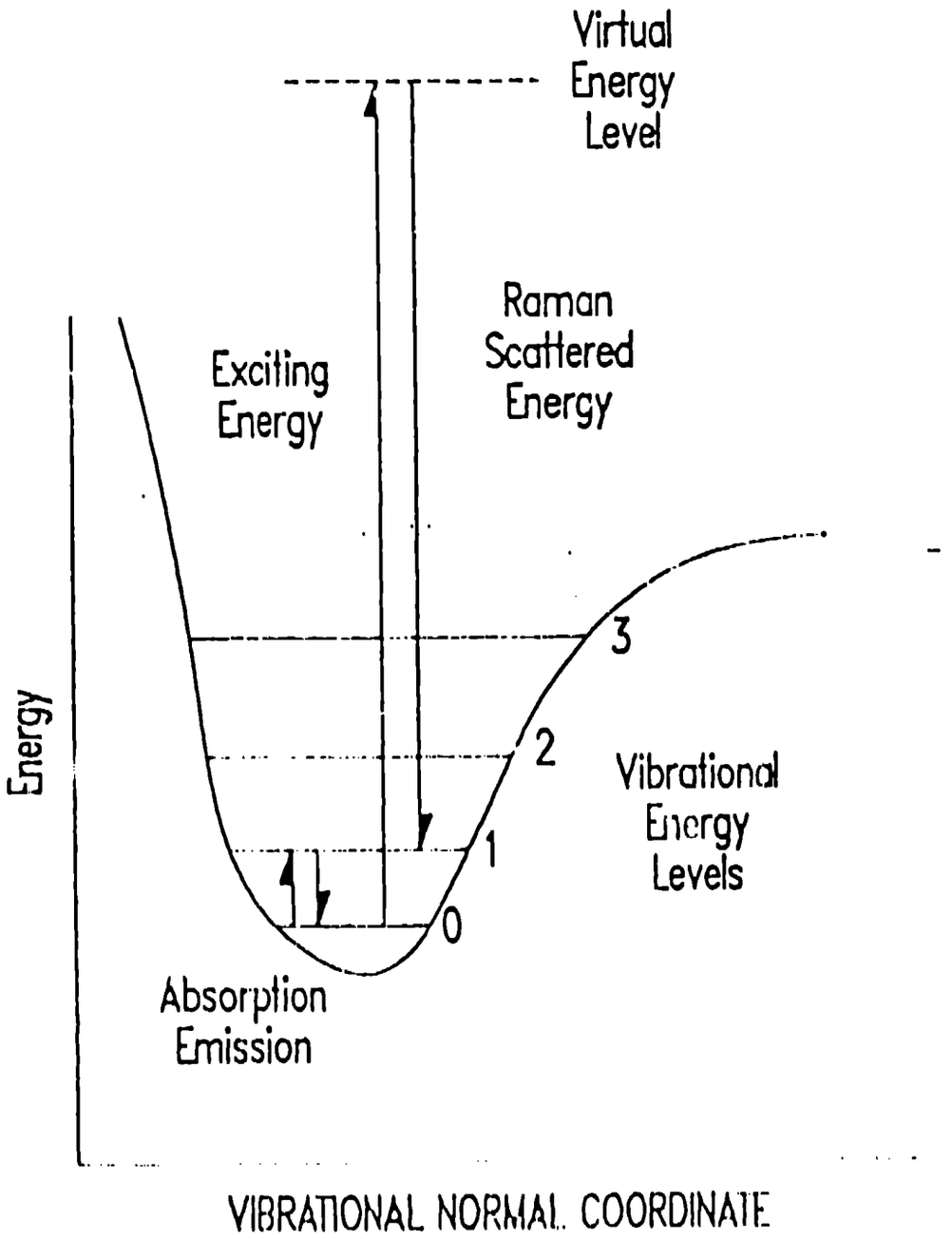

Figure 9.

STOKES, ANTI-STOKES INTENSITY RATIO

FROM BOISARD, TOMBINI AND MENIL

RAMAN SPECTRUM

FROM TAILLEUR AND CHERVILLE

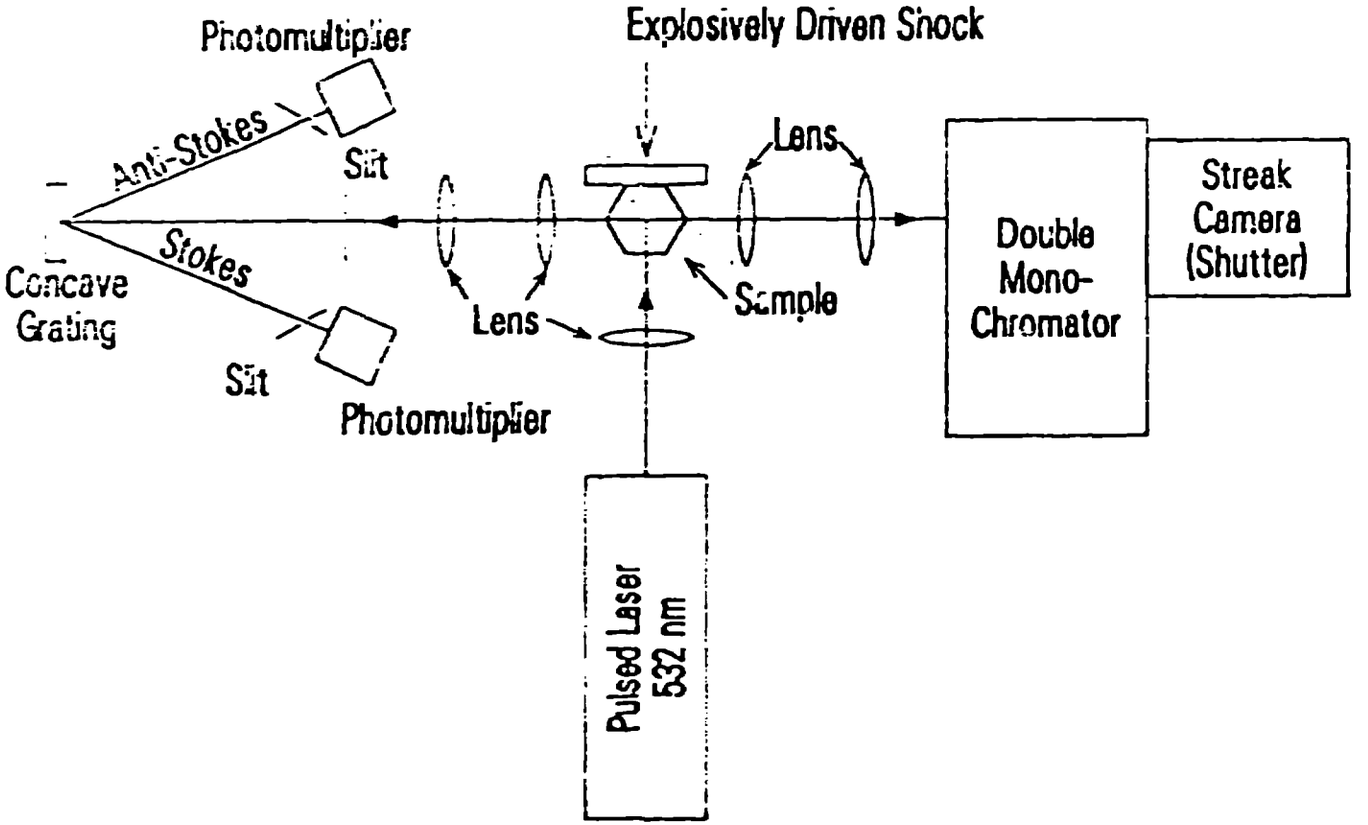

Figure 10.

COHERENT RAMAN SCATTERING

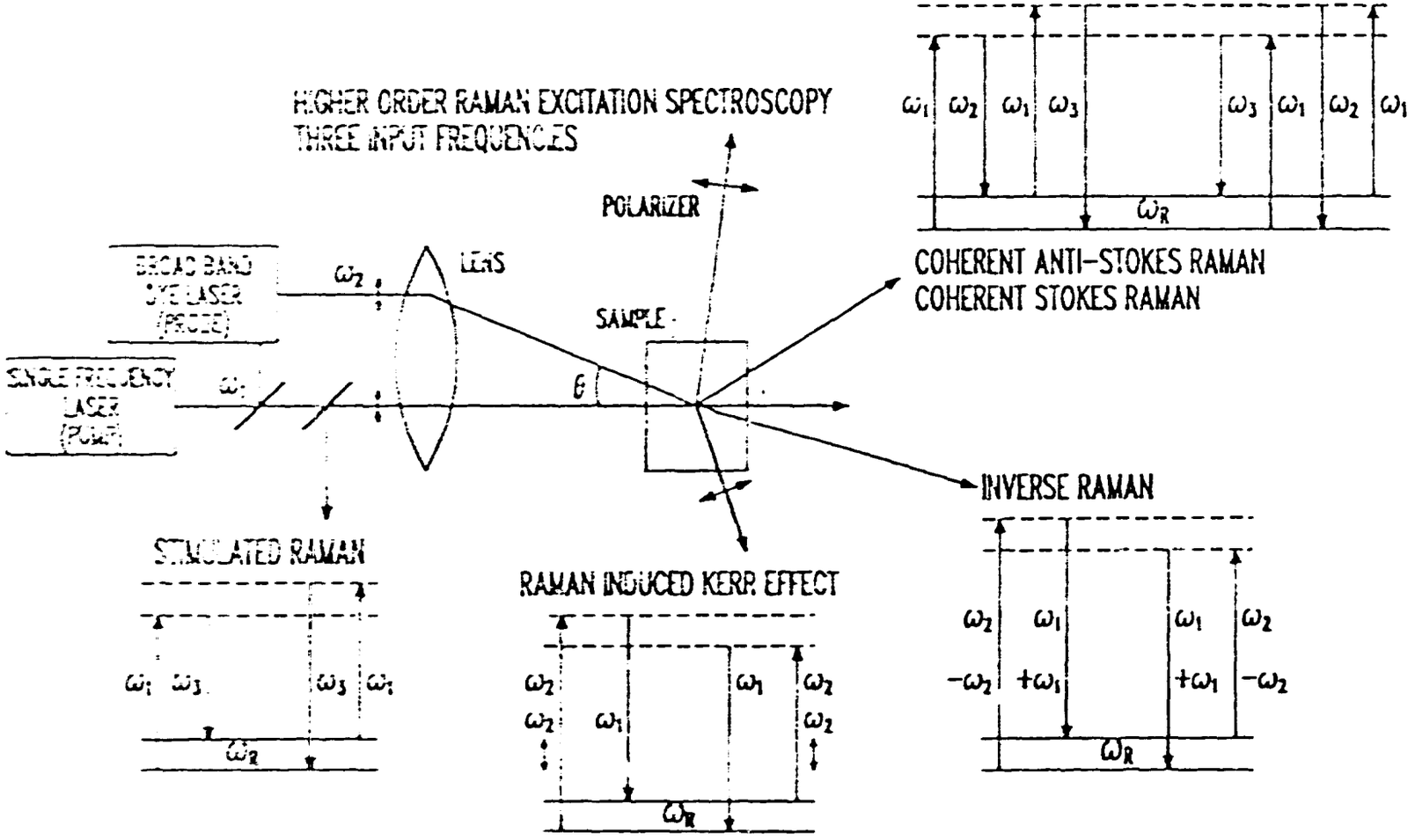

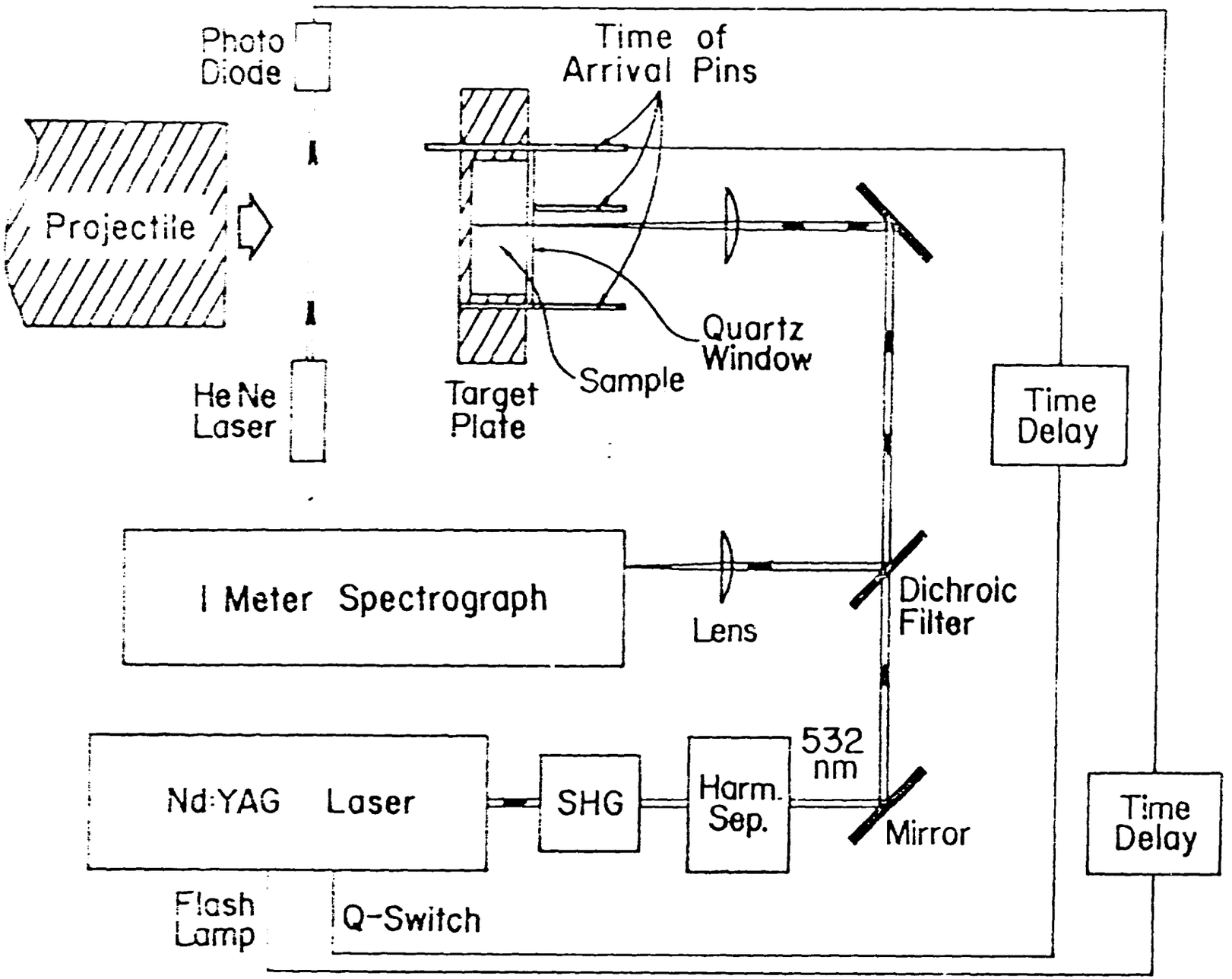
Photo Diode
Time of Arrival Pins
Projectile
Quartz Window
Sample
He Ne Laser
Target Plate
Time Delay
1 Meter Spectrograph
Lens
Dichroic Filter
532 nm
Nd:YAG Laser
SHG
Harm. Sep.
Mirror
Time Delay
Flash Lamp
Q-Switch

Figure 17.

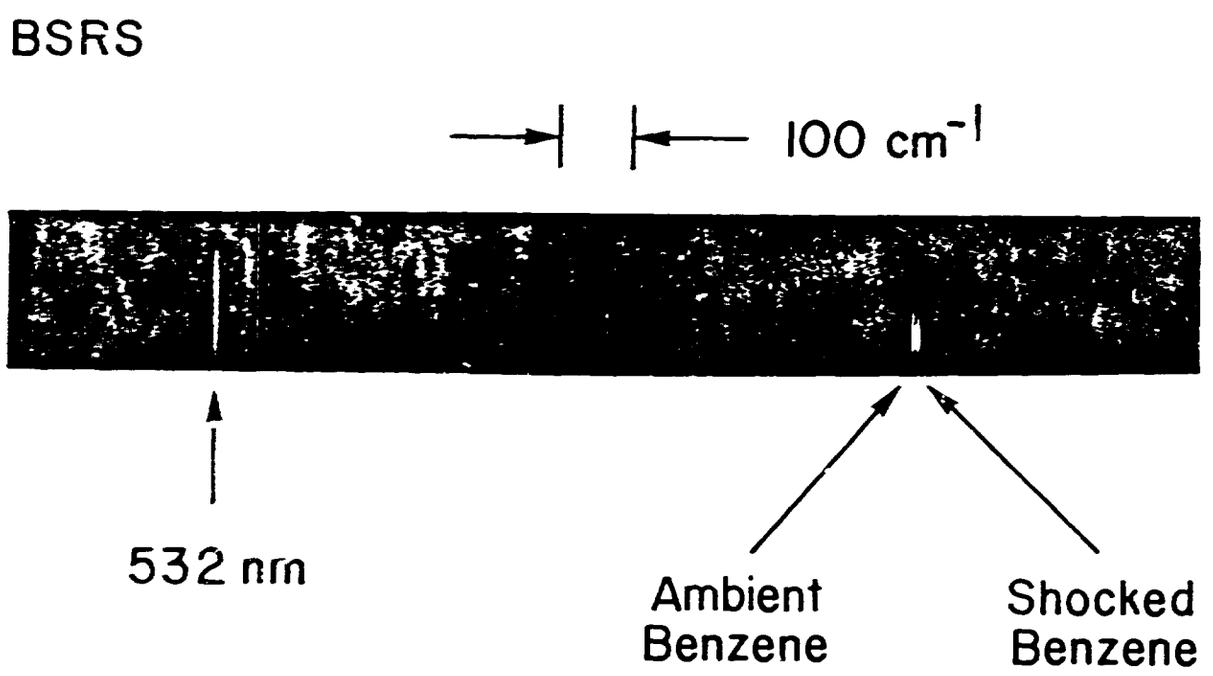

Figure 11.

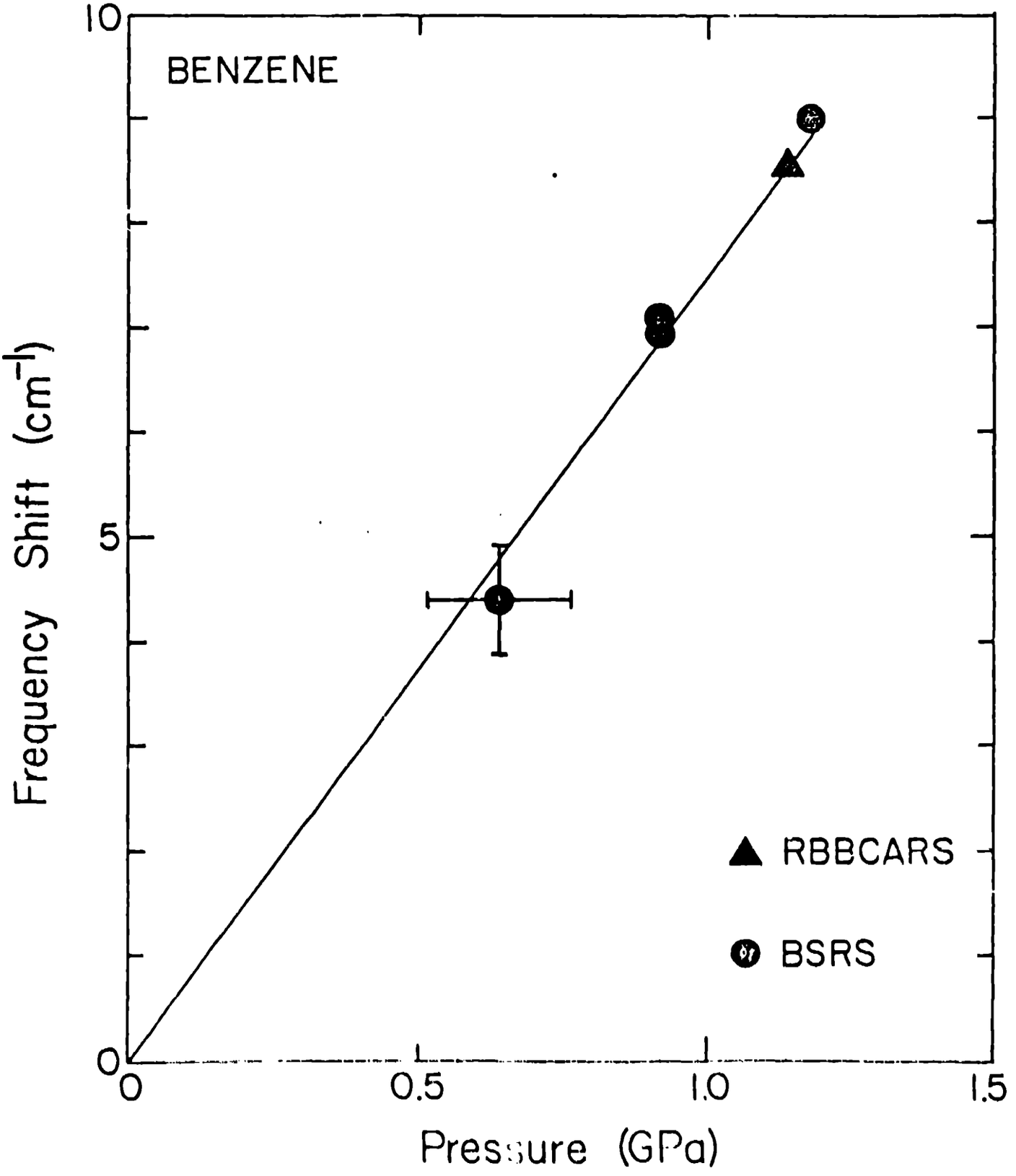
BENZENE
Frequency Shift (cm^{-1})
Pressure (GPa)
10
5
0
0
0.5
1.0
1.5
RBBCARS
BSRS

Figure 14.

INVERSE RAMAN AND RAMAN INDUCED KERR EFFECT

FROM VON HOLLE AND McWILLIAMS

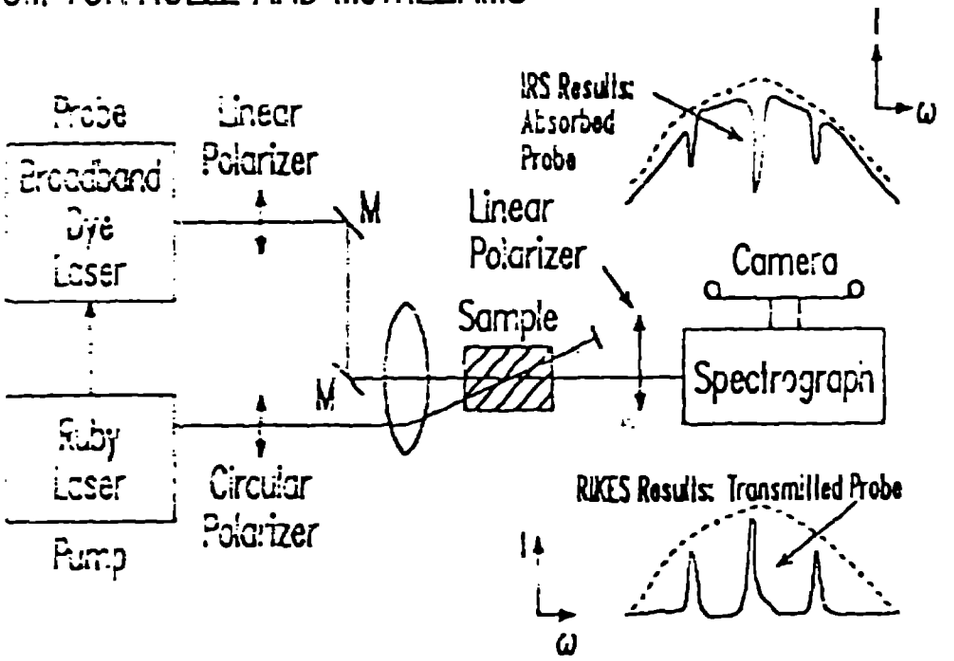

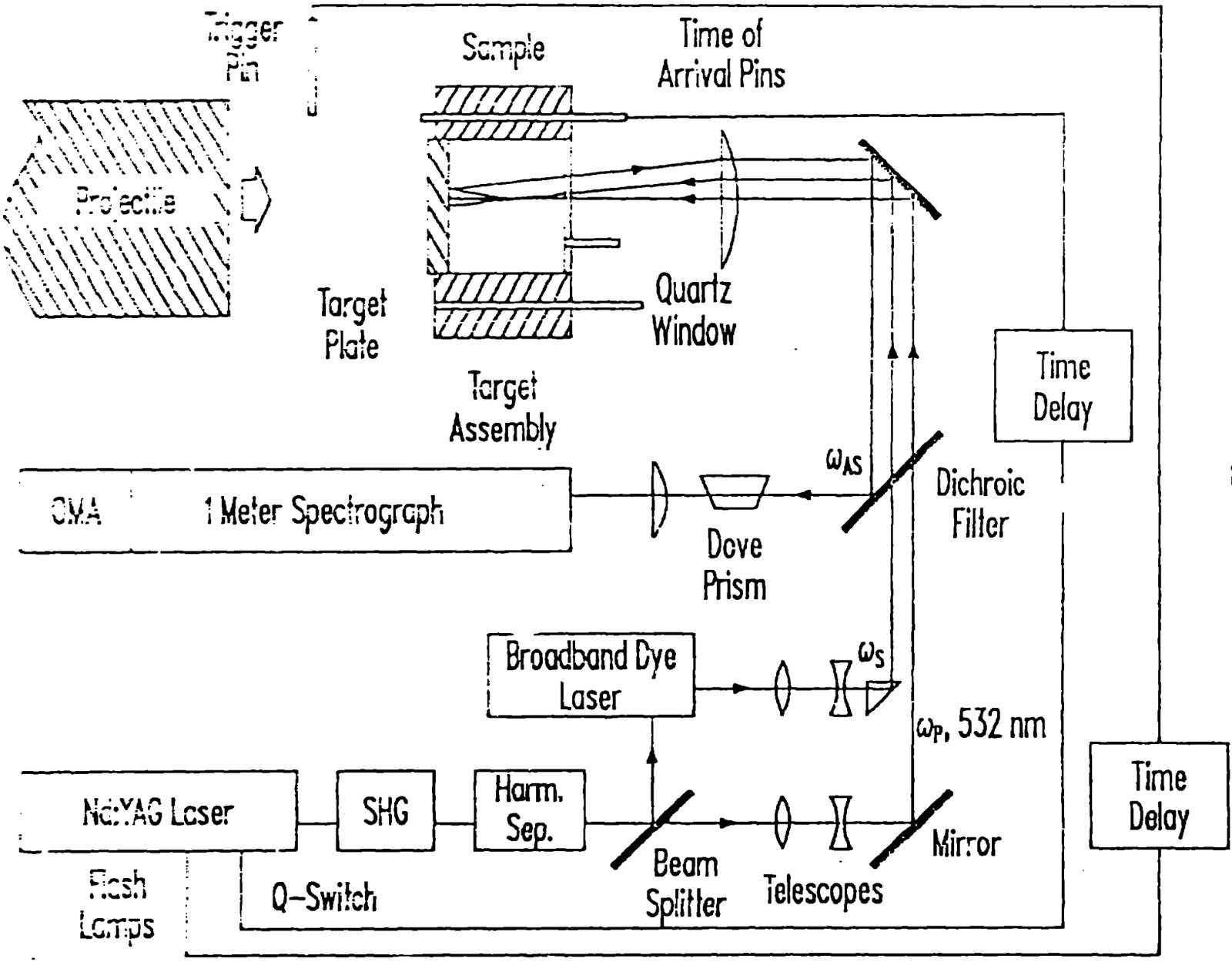
Trigger Pin
Sample
Time of Arrival Pins
Projectile
Target Plate
Quartz Window
Target Assembly
Time Delay
ω_{AS}
Dichroic Filter
OMA
1 Meter Spectrograph
Dove Prism
Broadband Dye Laser
ω_S
ω_P, 532 nm
Nd:YAG Laser
SHG
Harm. Sep.
Beam Splitter
Telescopes
Mirror
Time Delay
Flash Lamps
Q-Switch

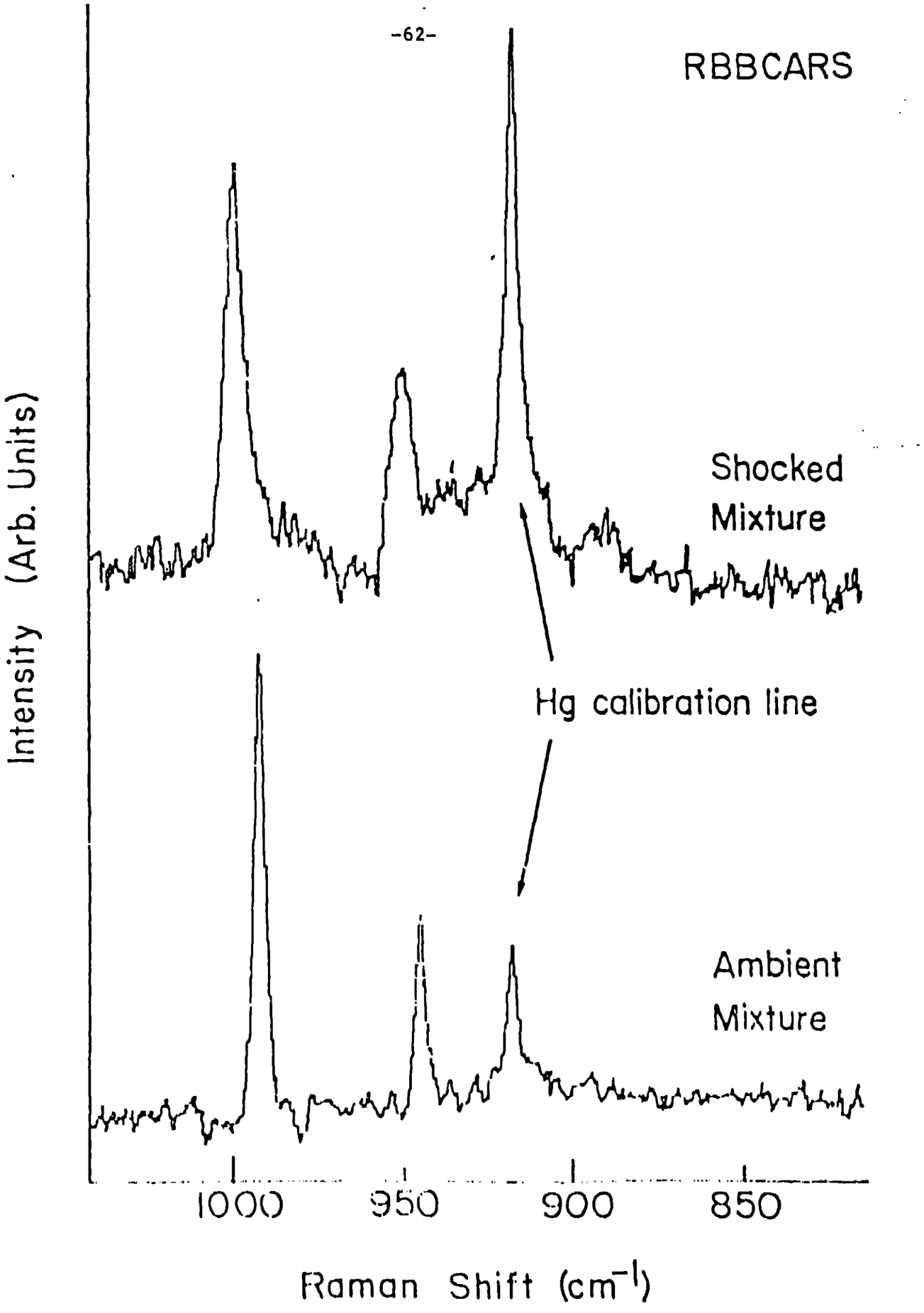
RBBCARS
Shocked
Mixture
Hg calibration line
Ambient
Mixture
Intensity (Arb. Units)
1000
950
900
850
Raman Shift (cm⁻¹)

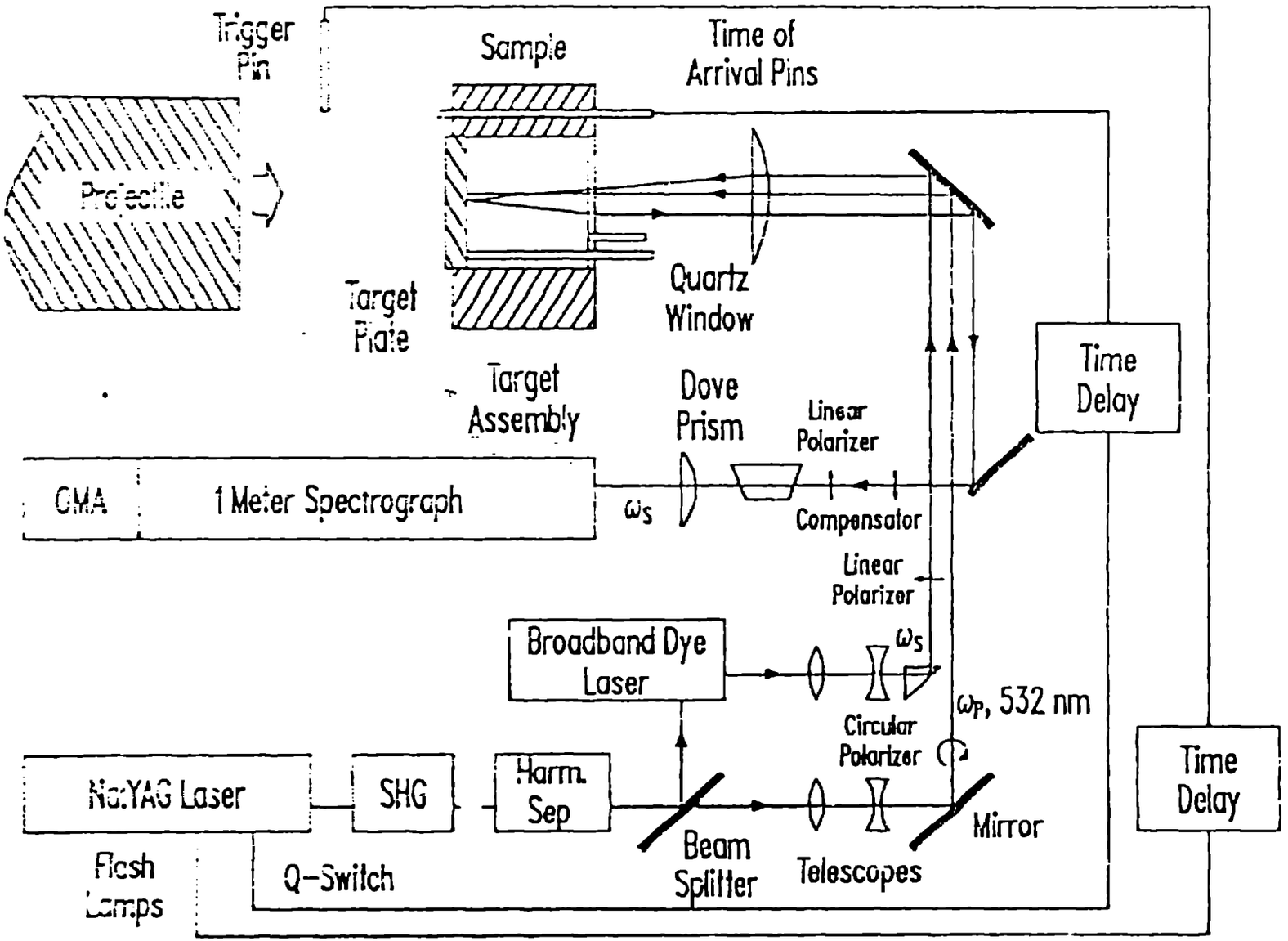
Trigger Pin
Sample
Time of Arrival Pins
Projectile
Target Plate
Quartz Window
Target Assembly
Dove Prism
Linear Polarizer
Time Delay
CMA
1 Meter Spectrograph
ω_S
Compensator
Linear Polarizer
Broadband Dye Laser
ω_S
ω_P, 532 nm
Circular Polarizer
Nd:YAG Laser
SHG
Harm. Sep
Beam Splitter
Telescopes
Mirror
Time Delay
Flash Lamps
Q-Switch

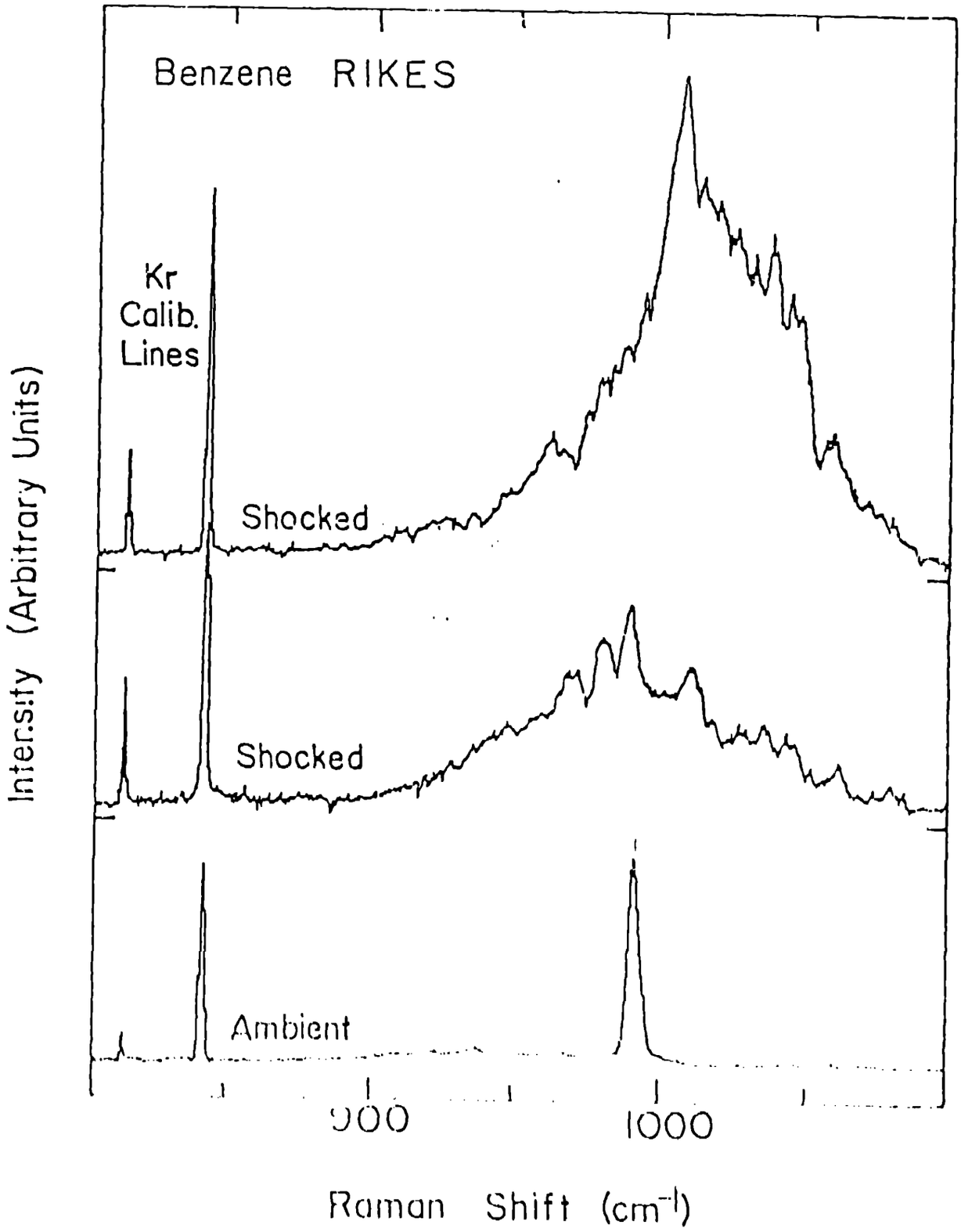
Benzene RIKES
Kr
Calib.
Lines
Shocked
Shocked
Ambient
Intensity (Arbitrary Units)
900
1000
Raman Shift (cm⁻¹)

Figure 19.

FAST X-RAY DIFFRACTION

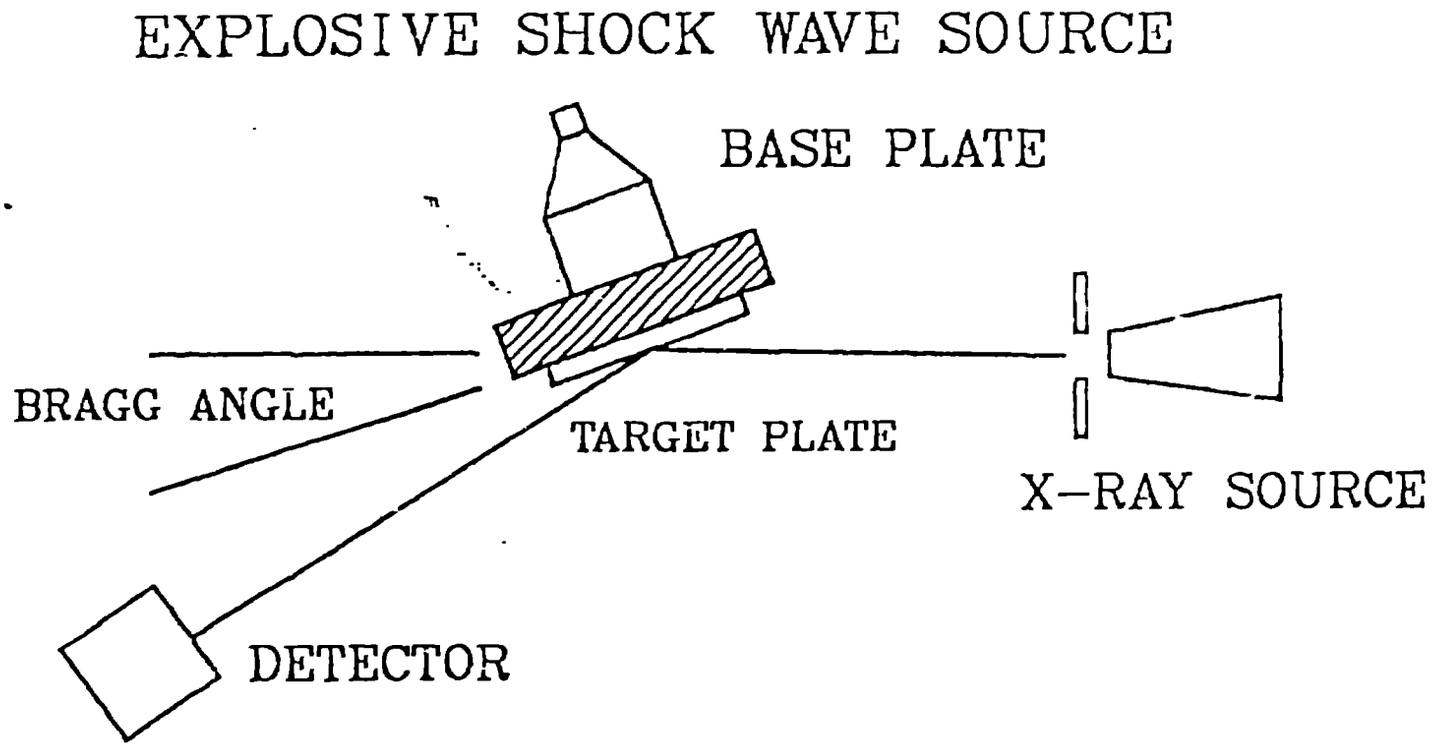

FROM JOHNSON, MITCHELL, KEELER AND EVANS

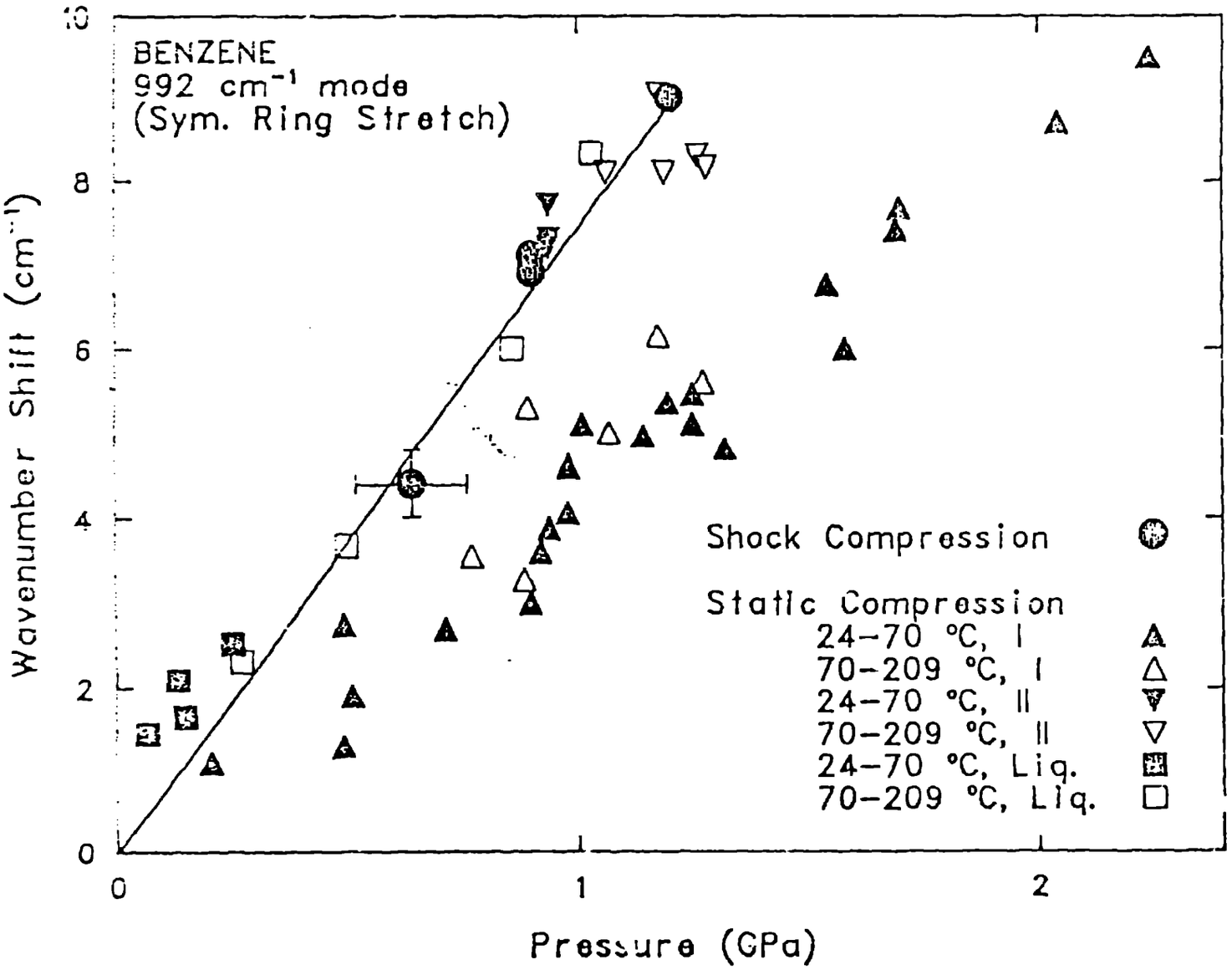
BENZENE
992 cm⁻¹ mode
(Sym. Ring Stretch)
Wavenumber Shift (cm⁻¹)
Pressure (GPa)
0
2
4
6
8
10
0
1
2
Shock Compression
Static Compression
24–70 °C, I
70–209 °C, I
24–70 °C, II
70–209 °C, II
24–70 °C, Liq.
70–209 °C, Liq.

Figure 21.

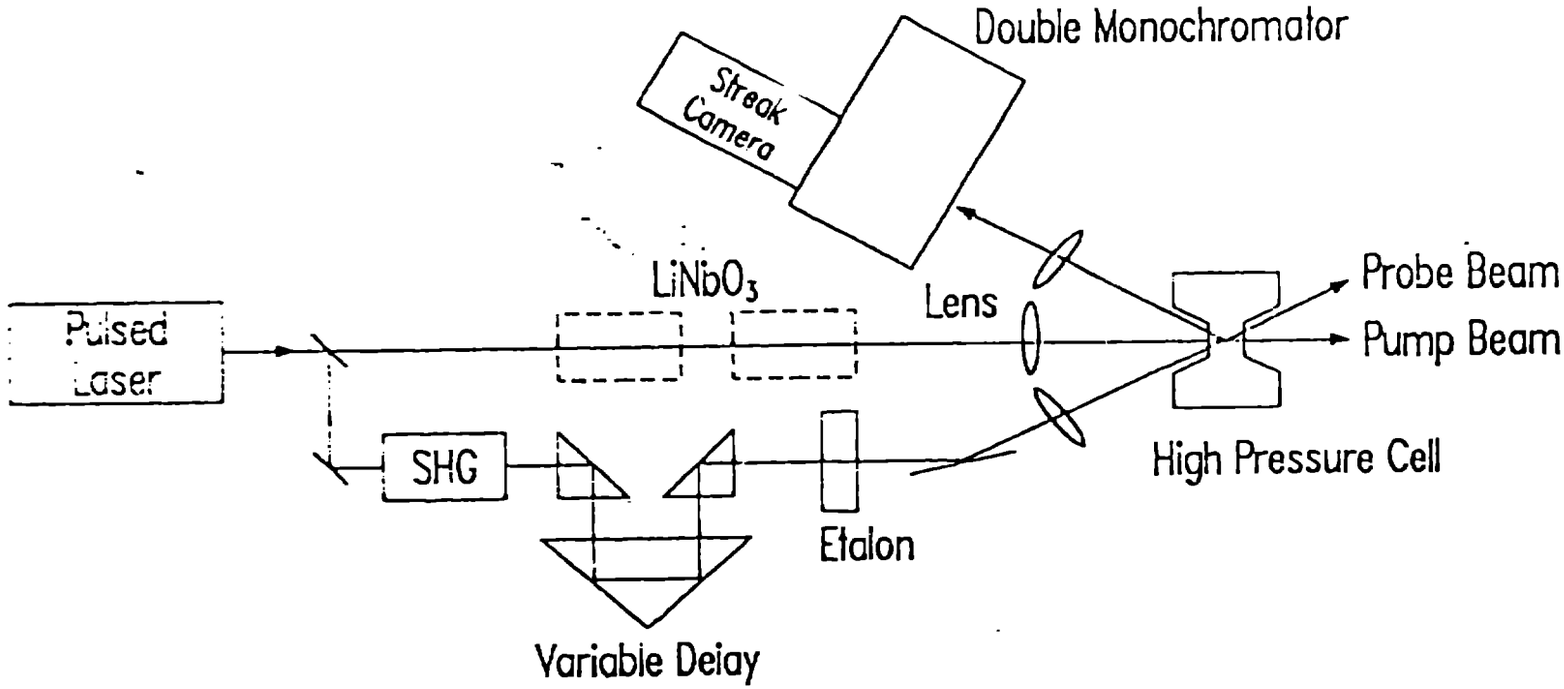
Double Monochromator
Streak Camera
LiNbO3
Lens
Probe Beam
Pump Beam
Pulsed Laser
SHG
High Pressure Cell
Etalon
Variable Delay

VIBRATIONAL ENERGY LEVELS AND INFRARED SPECTRUM: CH_2Cl_2

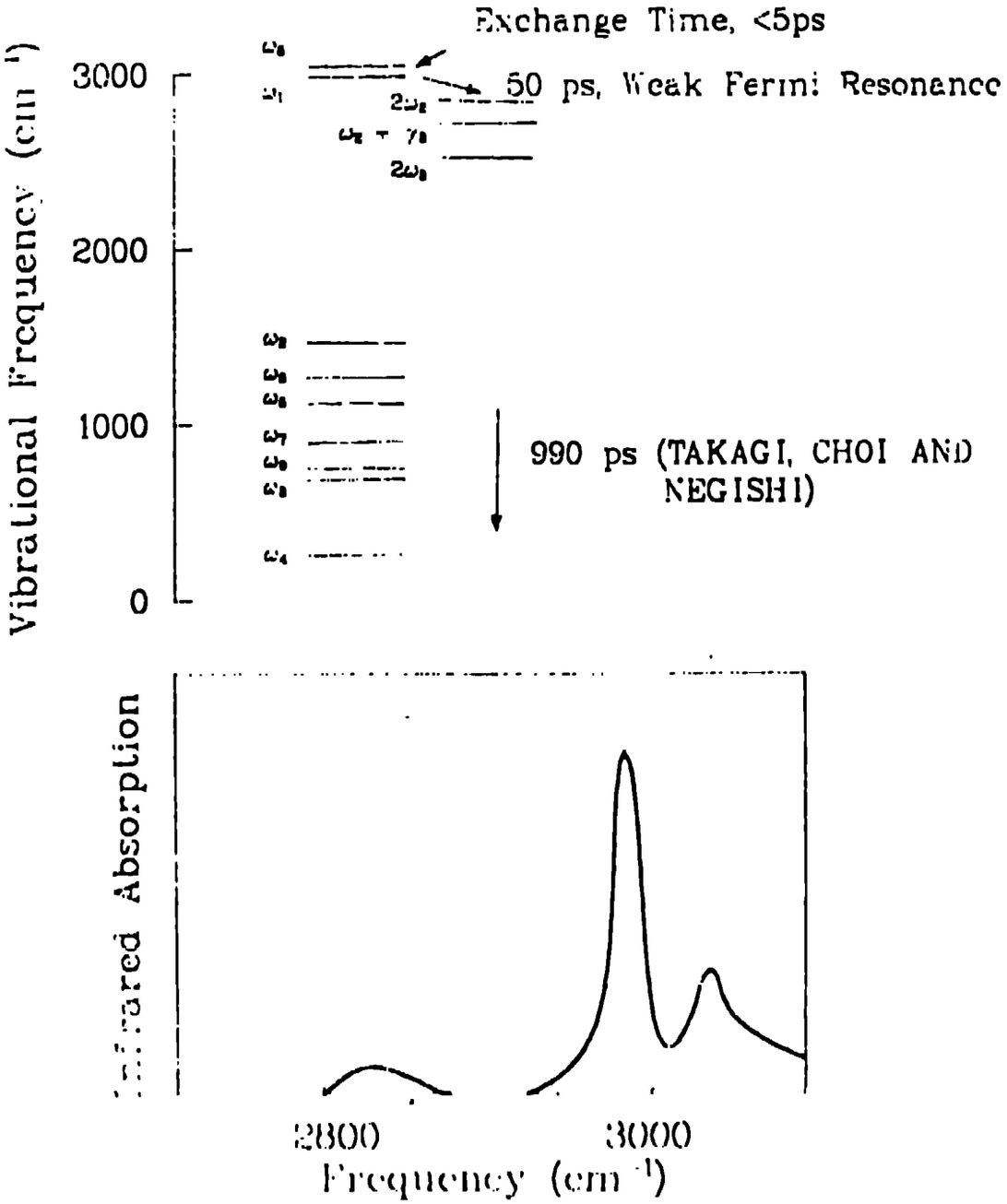

FROM LAUBEREAU, FISHER, SPANNER AND KAISER

Figure 21.